

Stable 3-level leapfrog integration in numerical relativity

Kimberly C. B. New

Department of Physics & Atmospheric Science, Drexel University, Philadelphia 19104

Keith Watt

Department of Astronomy, University of Maryland, College Park 20742-2421

Charles W. Misner

Department of Physics, University of Maryland, College Park 20742-4111

Joan M. Centrella

Department of Physics & Atmospheric Science, Drexel University, Philadelphia 19104
(*Physical Review D*, in press)

The 3-level leapfrog time integration algorithm is an attractive choice for numerical relativity simulations since it is time-symmetric and avoids non-physical damping. In Newtonian problems without velocity dependent forces, this method enjoys the advantage of long term stability. However, for more general differential equations, whether ordinary or partial, delayed onset numerical instabilities can arise and destroy the solution. A known cure for such instabilities appears to have been overlooked in many application areas. We give an improved cure (“deloused leapfrog”) that both reduces memory demands (important for 3 + 1 dimensional wave equations) and allows for the use of adaptive timesteps without a loss in accuracy. We show both that the instability arises and that the cure we propose works in highly relativistic problems such as tightly bound geodesics, spatially homogeneous spacetimes, and strong gravitational waves. In the gravitational wave test case (polarized waves in a Gowdy spacetime) the deloused leapfrog method was five to eight times less CPU costly at various accuracies than the implicit Crank-Nicholson method, which is not subject to this instability.

04.25.Dm, 04.30.Nk, 95.30.Sf

I. INTRODUCTION

Numerical relativity comprises the dynamical solution of the Einstein equations on a computer, allowing the construction of spacetimes that cannot be studied by purely analytic methods. A major application of numerical relativity is the modeling of astrophysical sources of gravitational radiation such as binary black hole [1] or neutron star inspiral [2], and nonspherical stellar collapse [3]. The continued development of gravitational wave detectors, with the expectation that ground-based interferometers such as LIGO [4], VIRGO [5] and GEO600 [6] will begin taking data in a few years, gives these studies a high priority. Numerical relativity is also important for studying the dynamics of pure gravitational waves [7], inhomogeneous cosmologies [8], the behavior of cosmological singularities [9,10], and critical behavior in general

relativity [11].

All of these endeavors require accurate numerical algorithms to correctly model the physics of curved spacetime. Simulations in three spatial dimensions plus time are expensive in terms of both CPU usage and memory requirements, and thus demand numerical methods that are efficient in both these regards. Memory limits, however, are less elastic in the short term than CPU time constraints. Thus a three-level second order algorithm may be more appropriate than a faster, high order algorithm which can only be implemented on smaller problems. Also, modeling the inspiral of binary black holes or neutron stars requires evolving the system for many orbital periods, so that numerical algorithms with long term stability and freedom from unphysical damping are essential.

Leapfrog methods are often used for the time integration of equations in numerical relativity and other branches of computational physics. The 3-level leapfrog method has the important property of being symplectic. In the context of a Hamiltonian system for which the differential equation has a symplectic structure (conjugate pairing of coordinates and momenta), this means that the difference equations also have such a structure and the integration step in the difference equations is a canonical transformation. With a symplectic integrator, all the Lagrangian integral invariants, including phase space volume, are exactly conserved by the integration scheme. Since the leapfrog method is time symmetric and maintains good conservation of physically conserved quantities [12–14], it has a well-deserved reputation in the context of Newtonian mechanics. Unfortunately this reputation is generally not merited when velocity dependent forces are met. In the integration of systems with such forces, this scheme is well-known to be susceptible to numerical instability (e.g., [15–19], and references therein), even under conditions where local linearization analysis anticipates stability. This instability occurs in the integration of both ordinary and partial differential equations and, in the case of partial differential equations, is independent of the mesh size used for the spatial

discretization [17].

An understanding of the origin of this instability was given by Sanz-Serna [17] who pointed out that the leapfrog scheme approximates not merely the intended differential equation system but a larger “augmented” system containing additional, nonphysical, parasitic modes. Since the leapfrog method is symplectic as applied to the augmented system [20], the advantages of symplectic methods (see [12]) would be attained to the extent that the parasitic modes remain zero numerically, as they do in an exact solution of the augmented system [21]. Aoyagi and Abe [18,22] identified the diagnostic symptom of this instability as a sawtooth oscillation or alternation of values between odd and even steps of the integration, and supplied a cure—a Runge-Kutta smoother to suppress this oscillation. Subsequent work [19] shows these phenomena in ordinary differential equations, where the delayed onset of this instability is clearly apparent.

We have studied the use of the 3-level leapfrog method in numerical relativity. In this work (see also [21]), we extend the ideas of Aoyagi and collaborators for removing the unstable parasitic modes, yielding an algorithm that reduces the number of time levels of data that must be stored by the code, allows the timestep to be changed, and thus is better suited to long-term integration of large scale numerical systems. Although we concentrate on the ADM 3+1 formalism for numerical relativity, our methods are quite general and thereby applicable to a wide range of problems in computational physics. Section II describes the source of the 3-level leapfrog instability. Section III presents our algorithm, dubbed “deloused leapfrog,” for removing instabilities that may arise in 3-level leapfrog integrations. In Sec. IV, we summarize the 3 + 1 formalism of numerical relativity and in Sec. V introduce three simple classes of Gowdy T^3 spacetimes. In Sec. VI, we use these models as relativistic testbeds for the deloused leapfrog technique and evaluate the numerical efficiency of deloused leapfrog by comparing its cost-effectiveness with those of the staggered leapfrog and Crank-Nicholson techniques. A summary and discussion of the results of the stability and efficiency tests of the deloused leapfrog technique is given in Sec. VII.

II. THE 3-LEVEL LEAPFROG INSTABILITY

We begin by considering the system of differential equations

$$\frac{d\mathbf{z}}{dt} = \mathbf{F}(\mathbf{z}, t). \quad (1)$$

Although we use a system of *ordinary* differential equations [Eqs. (1)] to describe the leapfrog instability and its cure in this section and the next, the techniques we outline apply equally well to systems of *partial* differential equations in which the time integration is carried out

using the leapfrog method; see Sec. VI below. The 3-level leapfrog discretization of this system is

$$\bar{\mathbf{z}}^{n+2} = \bar{\mathbf{z}}^n + 2\mathbf{F}(\bar{\mathbf{z}}^{n+1}, t^{n+1})\Delta t, \quad (2)$$

where we assume a constant timestep Δt between time levels n and $n+1$. The distinction between \mathbf{z} in the differential equation and $\bar{\mathbf{z}}$ in the difference equation is a warning that the relationship is not as straightforward as first appears. The discretization given in Eqs. (2) has $\mathcal{O}(\Delta t^2)$ accuracy and is a 3-level method, in that knowledge of data on time levels n and $n+1$ is needed to compute the result on time level $n+2$. The 3-level leapfrog algorithm [Eqs. (2)] is symplectic and time reversible, which means that it provides a Hamiltonian (damping free) model of an underlying Hamiltonian differential equation system [12,14].

Equations (1) arise in many physical applications in which \mathbf{z} comprises both position and velocity data $\mathbf{z} = (\vec{r}, \vec{v})$. For example, the motion of a particle of mass μ under the action of a force $\vec{f} = \mu\vec{a}$ is given by the set of equations

$$\begin{aligned} \frac{d\vec{r}}{dt} &= \vec{v} \\ \frac{d\vec{v}}{dt} &= \vec{a}, \end{aligned} \quad (3)$$

where \vec{r} is the position vector of the particle. The 3-level leapfrog discretization of Eqs. (3) gives

$$\begin{aligned} \vec{r}^{n+1} &= \vec{r}^{n-1} + 2\vec{v}^n \Delta t \\ \vec{v}^{n+1} &= \vec{v}^{n-1} + 2\vec{a}^n \Delta t \end{aligned} \quad (4)$$

For a particle moving in a Newtonian gravitational field $\vec{a}^n = \vec{a}^n(\vec{r}^n)$ and the system given by Eqs. (4) is stable and thus suitable for long time integrations. However, if there are so-called “velocity dependent forces” in which $\vec{a}^n = \vec{a}^n(\vec{r}^n, \vec{v}^n)$, such as arise for a particle moving under the influence of a magnetic field or a general relativistic gravitational field, the 3-level leapfrog scheme [Eqs. (4)] can become unstable. As we shall explain below, nonphysical parasitic modes can arise during the time integration and eventually destroy the numerical solution.

Notice that the leapfrog algorithm [Eqs. (2)] gives the value of $\bar{\mathbf{z}}^{n+2}$ at, say, the even time level $n+2$ in terms of the value $\bar{\mathbf{z}}^n$ at the even level n and the source term $\mathbf{F}(\bar{\mathbf{z}}^{n+1}, t^{n+1})$ at the odd level $n+1$. It also requires the specification of initial data at two time levels, $\bar{\mathbf{z}}^0$ and $\bar{\mathbf{z}}^1$, which is twice as much as the original first-order differential equation system requires. This doubling of initial condition specifications is the clue to the fact that this numerical algorithm using $\bar{\mathbf{z}}$ has twice as many degrees of freedom as does the physical system where states are specified by \mathbf{z} . The algorithm can be expressed, with a change of notation, by writing the solution at the even timesteps as $\bar{\mathbf{z}}^{2n} = \mathbf{x}^{2n}$ and at the odd timesteps as $\bar{\mathbf{z}}^{2n+1} = \mathbf{y}^{2n+1}$. With this, Eqs. (2) become

$$\begin{aligned} \mathbf{x}^{2n+2} &= \mathbf{x}^{2n} + 2\mathbf{F}(\mathbf{y}^{2n+1}, t^{2n+1})\Delta t \\ \mathbf{y}^{2n+3} &= \mathbf{y}^{2n+1} + 2\mathbf{F}(\mathbf{x}^{2n+2}, t^{2n+2})\Delta t \end{aligned} \quad (5)$$

Sanz-Serna [17] (concisely summarized in [23]) notes that Eqs. (5) can be considered to be a consistent single-step discretization of a larger system of equations for the even solutions \mathbf{x} and the odd solutions \mathbf{y} ,

$$\begin{aligned} \frac{d\mathbf{x}}{dt} &= \mathbf{F}(\mathbf{y}, t) \\ \frac{d\mathbf{y}}{dt} &= \mathbf{F}(\mathbf{x}, t), \end{aligned} \quad (6)$$

with timestep $2\Delta t$. Equations (6) are known as the augmented system [17,23].

If \mathbf{z} is a solution of Eqs. (1), it gives a solution of Eqs. (6), the augmented system, as $\mathbf{x} = \mathbf{z}$ and $\mathbf{y} = \mathbf{z}$. In general, however, other (unphysical) solutions will be possible. Since these unphysical, parasitic solutions can arise as valid solutions to the augmented difference system of Eqs. (5), the 3-level leapfrog integrator alone cannot distinguish between them and the physical solutions.

Since the physical solutions of Eqs. (6) have $\mathbf{x} = \mathbf{y}$ it is natural to define

$$\mathbf{x} = \mathbf{z} + \mathbf{w} \quad , \quad \mathbf{y} = \mathbf{z} - \mathbf{w} \quad , \quad (7)$$

so that the \mathbf{w} measure the parasitic deviations from the desired physical solutions \mathbf{z} . One can rewrite Eqs. (7) in finite difference form, using the definitions preceding Eqs. (5), as

$$\bar{\mathbf{z}}^n = \mathbf{z}^n + (-1)^n \mathbf{w}^n \quad . \quad (8)$$

The solution $\bar{\mathbf{z}}^n$ to the leapfrog difference system [Eqs. (2)] thus contains both physical \mathbf{z}^n and parasitic modes \mathbf{w}^n . With this notation, the augmented differential equations can be written as [19]

$$\begin{aligned} 2\frac{d\mathbf{z}}{dt} &= \mathbf{F}(\mathbf{z} - \mathbf{w}, t) + \mathbf{F}(\mathbf{z} + \mathbf{w}, t) \quad , \\ 2\frac{d\mathbf{w}}{dt} &= \mathbf{F}(\mathbf{z} - \mathbf{w}, t) - \mathbf{F}(\mathbf{z} + \mathbf{w}, t) \quad . \end{aligned} \quad (9)$$

We note that when these are expanded in powers of \mathbf{w} one has

$$\begin{aligned} \frac{d\mathbf{z}}{dt} &= \mathbf{F}(\mathbf{z}, t) + \mathcal{O}(\mathbf{w}^2) \quad , \\ \frac{d\mathbf{w}}{dt} &= -\mathbf{DF}(\mathbf{z}, t) \cdot \mathbf{w} + \mathcal{O}(\mathbf{w}^3) \end{aligned} \quad (10)$$

where \mathbf{DF} is the matrix of partial derivatives $\partial F_i / \partial z_j$.

The second of Eqs. (10), ignoring the cubic and higher terms, is a linear equation (in \mathbf{w}) which from the time dependence in $\mathbf{DF}(\mathbf{z}(t), t)$ easily gives rise to parametric amplification [24] leading to growth of the parasitic modes \mathbf{w} . Such parametric amplification was clearly diagnosed in a useful example [18]. A still stronger argument for the growth of parasitic modes (without the

above linear perturbation assumptions) had been given earlier by Sanz-Serna [17,23] based on his proof that the leapfrog scheme preserves volume in the augmented state space even when the original system is not Hamiltonian. Sanz-Serna has an elementary example, $dz/dt = z^2$, $z(0) = -1$, with a two dimensional zw augmented phase space (Fig. 1 in [17]); this shows all the qualitative features of the delayed onset instability typical of numerical catastrophies that generally result from using leapfrog in nonlinear systems with velocity dependent forces. In this example, *every* solution diverges ($z \rightarrow \infty$) if at any point $w \neq 0$, although $z \rightarrow 0$ as $t \rightarrow \infty$ for the physical $w = 0$ solution. Numerical experiments with leapfrog follow the divergent solutions of this analytical example since $w \neq 0$ at some point arises either from imperfect initial conditions, roundoff error, or discretization error. Hence, nonlinear interaction or parametric amplification of linear interaction between the physical and parasitic modes of the solution to the leapfrog difference system [Eqs. (2)] can cause the parasitic mode to grow to the point where it destroys the numerical solution.

However, if the augmented difference system [Eqs. (2) or (5)] decouples, no such instability occurs. To illustrate what it means for these equations to decouple, consider the augmented difference system for Eqs. (4), in the absence of velocity dependent forces. In that case one can let $\mathbf{x} = (\vec{r}, \vec{u})$ and $\mathbf{y} = (\vec{q}, \vec{v})$ to find that the (even \vec{r} , odd \vec{v}) system does not couple to the (odd \vec{q} , even \vec{u}) system. Thus the augmented difference system consists of two interlaced, noninteracting copies (even \vec{r} , odd \vec{v}) and (odd \vec{q} , even \vec{u}) of the physical system. Each of these two systems is of the Newtonian form where the leapfrog scheme has shown itself remarkably stable.

Thus, as mentioned above, in a 3-level leapfrog integration of Eqs. (3) stability can generally only be anticipated in the absence of velocity dependent forces. In this case, the parasitic mode is generally still present as the difference between two interlaced numerical solutions of Eqs. (3), but will remain small unless the physical system is highly sensitive to small differences in initial conditions (i.e., chaotic). Note that it is customary, in the absence of velocity dependent forces, to omit the \vec{q} and \vec{u} variables from the integration scheme, yielding the staggered leapfrog scheme (see below). Alternatively, in a code based on Eqs. (2), one could in this case solve for two independent solutions approximating Eqs. (1) based on distinct initial conditions for (\vec{r}, \vec{v}) and for (\vec{q}, \vec{u}) .

A stable 3-level leapfrog integration of a system of equations containing “velocity dependent forces” can be maintained if the growth of the parasitic mode can be controlled. When a constraint $\mathbf{w} = \mathbf{0}$ is adjoined to Eqs. (9) they reduce to the original physical system of Eq. (1). This constraint, when imposed initially, is preserved by the differential equation system (9) since $\mathbf{w} = \mathbf{0}$ gives $d\mathbf{w}/dt = 0$. But in numerical implementations errors will inevitably introduce nonzero \mathbf{w} . The cure proposed by Aoyagi and Abe [18,22] is to reimpose the constraint $\mathbf{w} = \mathbf{0}$ as necessary to suppress the parasitic

mode. Their method for doing so is based on the identification of \mathbf{w} via its signature even-odd timestep alternation in sign, which is evident in Eq. (8). As noted in [21], this method is very efficient since, from the power series expansions in Eqs. (10), the parasitic modes \mathbf{w} need merely be suppressed to single precision accuracy to assure that they do not contaminate the physical solution \mathbf{z} in double precision. We will return to the cure in Sec. III below.

Note that the instability under discussion here is not related to the “mesh-drifting” instability inherent to non-dissipative leapfrog integrations of partial differential equations [25]. As has been emphasized above, the 3-level leapfrog instability can arise in integrations of both ordinary and partial differential equations and results from the temporal, not spatial, discretization of the method.

To demonstrate this instability, we have used the 3-level leapfrog method to numerically integrate the geodesic equations for a particle moving on a circular orbit of radius r_0 in the Schwarzschild spacetime. In the limit $r_0 \gg M$, we recover the usual Newtonian equations of motion [Eqs. (3)]. In this case, the leapfrog method produced a circular orbit that was stable for ten thousand orbital periods (before we terminated the run). However, as r_0 is decreased, general relativistic effects give rise to terms that behave like velocity-dependent forces and the integrator fails to maintain a stable evolution. Fig. 1 shows the results of the geodesic integration for the case $r_0 = 10M$. The particle orbit shown in Fig. 1a initially appears to be stable; eventually the instability manifests as the solutions on the even and odd timesteps diverge. Fig. 1b shows the magnitude of the particle’s position vector as a function of time; again the even and odd solutions clearly diverge as the parasitic mode grows to destructive levels. Although the parasitic mode is present from the beginning of the calculation, it takes a number of orbits before it grows to noticeable levels; the instability then grows catastrophically, causing the integration to crash after about six orbits.

Two other integration methods (whose efficiency we will compare with that of our deloused leapfrog algorithm in Sec. VI), staggered leapfrog and Crank-Nicholson, do not suffer from the instability present in the 3-level leapfrog algorithm. In both cases this happens because neither of these algorithms augments the phase space (or state space) of the problem by adding new degrees of freedom not found in the physical system. To illustrate this, we will continue to use the integration of Eqs. (3) as the example upon which we base our outline of these integration algorithms.

As mentioned above, the even and odd degrees of freedom in Eqs. (3) can be written $\mathbf{x} = (\vec{r}, \vec{u})$ and $\mathbf{y} = (\vec{q}, \vec{v})$. But when the force law lets $\vec{a} = \vec{a}(\vec{r})$ be calculated independently of \vec{v} , the (\vec{r}, \vec{v}) pair of variables are not coupled to the (\vec{q}, \vec{u}) pair, so this second pair can be dropped from the numerical algorithm. This leads to the methodology of the staggered leapfrog algorithm, which defines the variables it evolves on alternating time levels only. A

staggered leapfrog integration of Eqs. (3) would, for example, evaluate only \vec{r} at even steps and only \vec{v} at odd steps. It is then customary to renumber the steps so that the even steps are integer values, the odd half integer:

$$\begin{aligned}\vec{r}^{n+1} &= \vec{r}^n + \vec{v}^{n+1/2} \Delta t \\ \vec{v}^{n+3/2} &= \vec{v}^{n+1/2} + \vec{a}^{n+1} \Delta t\end{aligned}\quad , \quad (11)$$

where the constant Δt is the difference between two consecutive integer (or half-integer) time levels [25]. The initial conditions are specified by giving $(\vec{r}^0, \vec{v}^{1/2})$. This method is time-symmetric and symplectic and thus avoids nonphysical damping [12,13]. Here, with velocity independent Newtonian forces, one has a 2-level method. [I.e., only the \vec{v} components are used in updating the \vec{r} ’s, and only the \vec{r} components in updating the \vec{v} ’s.] This leapfrog method gives second order accuracy at the same computational cost as the first order Euler method.

When \vec{a} depends on \vec{v} as well as \vec{r} , a method such as extrapolation (e.g., $\vec{v}^{n+1} = (3/2)\vec{v}^{n+1/2} - (1/2)\vec{v}^{n-1/2}$) is needed to calculate \vec{v} at the integer (or even) levels; this generally destroys the time-symmetric nature of the algorithm and leads to errors in conserved quantities.

The Crank-Nicholson technique is an iterative integration algorithm [26]. For the system given in Eqs. (3), the iteration cycle is initialized by setting

$$\vec{r}^{n+1} = \vec{r}^n, \quad \vec{v}^{n+1} = \vec{v}^n. \quad (12)$$

Then data at the half integer levels $n + 1$ is determined via

$$\begin{aligned}\vec{r}^{n+1/2} &= \frac{1}{2}(\vec{r}^{n+1} + \vec{r}^n) \\ \vec{v}^{n+1/2} &= \frac{1}{2}(\vec{v}^{n+1} + \vec{v}^n)\end{aligned}\quad . \quad (13)$$

Next, the values of the data at level $n + 1$ are updated according to

$$\begin{aligned}\vec{r}^{n+1} &= \vec{r}^n + \vec{v}^{n+1/2} \Delta t \\ \vec{v}^{n+1} &= \vec{v}^n + \vec{a}^{n+1/2} \Delta t\end{aligned}\quad , \quad (14)$$

where $\vec{a}^{n+1/2}$ has been computed based on the data given by Eqs. (13). The steps given by Eqs. (13) and (14) are then repeated until the relative differences of the values of each of the components of \vec{r}^{n+1} and \vec{v}^{n+1} between adjacent iteration cycles have each converged to the desired level of accuracy. This method requires the specification of initial data \vec{r}^0 and \vec{v}^0 . It has accuracy $\mathcal{O}(\Delta t^2)$; it is time symmetric if the iteration converges to machine precision.

Both the staggered leapfrog and the Crank-Nicholson algorithms avoid the instability arising from an augmented phase space. One sees in each case that there is a single physical pair of values at each timestep. These are $(\vec{r}^n, \vec{v}^{n+1/2})$ for staggered leapfrog and (\vec{r}^n, \vec{v}^n) for Crank-Nicholson. Other quantities such as \vec{v}^{n+1} in staggered leapfrog or the half integer values in Crank-Nicholson are temporary variables computed from the physical data. Thus no extraneous degrees of freedom, like the \mathbf{w} quantities in 3-level leapfrog, appear.

III. DELOUSED LEAPFROG

The instability in the 3-level leapfrog scheme is ideally eliminated with a technique that retains as much of the symplectic character of the 3-level scheme as possible. Aoyagi and Abe [18,22] give such a prescription to remove the parasitic modes before they grow large enough to destroy the calculation. This method relies on the Runge-Kutta (RK) method [25] and is called the RK smoother. (The usual RK algorithm is fourth order; however, Aoyagi and Abe do not state what order RK scheme is used in their smoother.) They compare it to a less effective second order smoother suggested by a colleague. We have extended the work of Aoyagi and Abe to produce a second order algorithm which requires less storage and also allows the use of adaptive (i.e., not constant in time) timesteps Δt (see also [21]). We term the 3-level method with this improved smoother “deloused leapfrog,” since it removes the parasitic modes from the calculation. In this section, we give the algorithm for this deloused leapfrog method. Ref. [21] discusses its properties in Hamiltonian problems with applications to highly noncircular and highly relativistic geodesics. Those applications use the adaptive timestep our delousing routine allows.

The prescription for a delousing step to remove the parasitic modes uses a second order Runge-Kutta (RK2) algorithm. (The usual RK algorithm is fourth order.) Our algorithm proceeds as follows. Referring to the 3-level discretization in Eq. (4), we assume that data is available on (say) an odd level n and an even level $n - 1$. First, use RK2 to evolve the data a half-step backward from the odd level n and a half-step forward from the even level $n - 1$:

Step (1) use RK2 with $\delta t = -\frac{1}{2}\Delta t$
to get $\vec{r}_{odd}^{n-1/2}, \vec{v}_{odd}^{n-1/2}$ from \vec{r}^n, \vec{v}^n

Step (2) use RK2 with $\delta t = +\frac{1}{2}\Delta t$
to get $\vec{r}_{even}^{n-1/2}, \vec{v}_{even}^{n-1/2}$ from $\vec{r}^{n-1}, \vec{v}^{n-1}$,

where, for example, $\vec{r}_{odd}^{n-1/2}$ represents data on level $n - \frac{1}{2}$ that comes from the odd level n . We now have data from both odd and even solutions at the same time level $n - \frac{1}{2}$. Eqs. (7) are then utilized to obtain the data $\vec{r}^{n-1/2}$ and $\vec{v}^{n-1/2}$ that contain only the physical mode:

Step (3) set $\vec{r}^{n-1/2} = \frac{1}{2}(\vec{r}_{even}^{n-1/2} + \vec{r}_{odd}^{n-1/2})$,
 $\vec{v}^{n-1/2} = \frac{1}{2}(\vec{v}_{even}^{n-1/2} + \vec{v}_{odd}^{n-1/2})$.

With the parasitic mode thus eliminated at level $n - \frac{1}{2}$ (i.e., with the constraint $\mathbf{w} = 0$ enforced), we now use RK2 to step the data a half-step forward and backward:

Step (4) use RK2 with $\delta t' = +\frac{1}{2}\Delta t'$
to get \vec{r}^n, \vec{v}^n from $\vec{r}^{n-1/2}, \vec{v}^{n-1/2}$

Step (5) use RK2 with $\delta t' = -\frac{1}{2}\Delta t'$
to get $\vec{r}^{n-1}, \vec{v}^{n-1}$ from $\vec{r}^{n-1/2}, \vec{v}^{n-1/2}$.

Since RK2 does not suffer from the leapfrog instability (for the same reason as that given in the preceding section for the stability of the staggered leapfrog and Crank-Nicholson methods), no parasitic mode is introduced by its use. With this “deloused” data at levels n and $n - 1$, which contain only the physical modes, the 3-level leapfrog integration is resumed. This prescription can be coded so that no more than three levels of data for \vec{r} and \vec{v} need be kept in memory at any one time, which is an important consideration when it is applied to 3 + 1 dimensional partial differential equations.

Steps (4) and (5) of this procedure can also be used to start the integration. With initial data specified (e.g., at $t = 0$) as values for $\vec{r}^{1/2}, \vec{v}^{1/2}$, this procedure provides \vec{r}^0, \vec{v}^0 and \vec{r}^1, \vec{v}^1 to start the 3-level algorithm of Eqs. (2).

Notice that the timesteps $\pm\frac{1}{2}\Delta t'$ used in Steps (4) and (5) to bring the deloused data from level $n - \frac{1}{2}$ to levels n and $n - 1$ are not required to be the same as the timesteps $\pm\frac{1}{2}\Delta t$ used in Steps (1) and (2). This is an improvement on the method of Aoyagi and Abe [18,22] and allows the system timestep to be changed whenever delousing is performed, with the integration restarted in a time symmetric manner. In this paper, all our runs were carried out using constant timesteps; see, however, Ref. [21] for an example of adaptive timesteps applied to highly eccentric particle orbits.

The deloused leapfrog method is not strictly symplectic because the delousing steps are taken using RK2, which is not a symplectic method, and the suppression Step (3) does not preserve volume in the augmented phase space. Since delousing steps can in principle be rare, and ideally do not disturb the physical solution (when the $\mathcal{O}(\mathbf{w}^2)$ terms in Eqs. (10) are beyond machine precision), the failure here of the time symmetric and symplectic properties possessed by Eqs. (2) could have negligible impact.

To determine when a delousing step is needed, the growth of the parasitic mode is monitored. Since Eq. (7) shows that this parasitic mode changes sign on each time level n , we look for this alternate timestep oscillation in some quantity that characterizes the system. The detection of such an oscillation in the quantity monitored triggers a call to the delousing module, which then removes the parasitic mode. The goal is to monitor a quantity that manifests the instability at detectable levels early enough, so that it can be eliminated before it dominates the integration. The best quantity to use for the delousing trigger varies from problem to problem and also depends on what level of parasitic mode one is willing to tolerate in the solution (see further discussion in Secs. VI and VII).

Figure 2 shows the results of our deloused leapfrog integration of the same particle equations of motion as in Fig. 1. The delousing trigger chosen in this case was an oscillation in a quantity based upon the action $dJ = \frac{1}{2}(p dq - q dp)$ of Hamiltonian mechanics:

$$\Delta J = \frac{1}{2}(\vec{p}^n + \vec{p}^{n-1}) \cdot (\vec{r}^n - \vec{r}^{n-1})$$

$$\begin{aligned}
& -\frac{1}{2}(\vec{r}^n + \vec{r}^{n-1}) \cdot (\vec{p}^n - \vec{p}^{n-1}) \\
& = \vec{r}^n \cdot \vec{p}^{n-1} - \vec{p}^n \cdot \vec{r}^{n-1},
\end{aligned} \tag{15}$$

where \vec{r} and \vec{p} are the particle's position and momentum vectors, respectively. The use of this trigger initiated a delousing step about once every 405 timesteps. The orbit was stable for the duration of our simulation, about ten thousand orbits.

IV. THE 3 + 1 FORMALISM OF NUMERICAL RELATIVITY

The development of the deloused leapfrog algorithm described in the preceding section was motivated by our search for a stable and efficient time integration technique that could be utilized in CPU and memory intensive, general relativistic simulations of the orbital stability of binary neutron stars. This section briefly summarizes the 3 + 1 form of the Einstein equations upon which such numerical relativity simulations are based. Here we consider only vacuum spacetimes; however, our results apply to models with sources as well.

The Einstein field equations of general relativity are $G_{\mu\nu} = 8\pi T_{\mu\nu}$, where $G_{\mu\nu}$ and $T_{\mu\nu}$ are the Einstein and stress energy tensors, respectively [27]. We set $T_{\mu\nu} = 0$ (as is the case for vacuum spacetimes), $G = c = 1$ and our convention is such that Greek indices run from 0 to 3, Latin indices run from 1 to 3, and repeated raised and lowered indices are summed over. The numerical solution of the Einstein equations is facilitated by the ADM decomposition [27,28], which divides four dimensional spacetime into a series of three dimensional, space-like slices that are connected by one dimensional, timelike curves. This “3+1” split transforms the Einstein equations into two sets: the evolution equations, which govern temporal changes in the gravitational field variables, and the constraint equations, which the field variables must satisfy on each spacelike slice.

The general form of the metric in the ADM formalism is

$$ds^2 = -(\alpha dt)^2 + g_{ij}(dx^i + \beta^i dt)(dx^j + \beta^j dt). \tag{16}$$

The vacuum evolution equations for the three-metric g_{ij} and the extrinsic curvature K_{ij} are (see, e.g., [29] and references therein)

$$g_{ij,t} = -2\alpha K_{ij} + D_i\beta_j + D_j\beta_i, \tag{17}$$

and

$$\begin{aligned}
K_{ij,t} &= -D_i D_j \alpha + \beta^l D_l K_{ij} + K_{il} D_j \beta^l + K_{lj} D_i \beta^l \\
&+ \alpha [R_{ij} - 2K_{il} K_j^l + K K_{ij}],
\end{aligned} \tag{18}$$

where t is coordinate time, commas denote partial derivatives, $K = K_i^i$, and D_i and R_{ij} are the covariant derivative and Ricci tensor, respectively, formed from the three-metric g_{ij} . The lapse α and the shift vector β^i are freely

specifiable and define the coordinate conditions under which g_{ij} and K_{ij} are evolved. The right hand side of Eq. (17) may be a function of g_{ij} , as dependence on g_{ij} arises through the covariant derivative operation when β^i is nonzero or when α is chosen to depend on g_{ij} ; moreover, the right hand side of Eq. (18) is always a function of K_{ij} . Thus “velocity dependent forces” are generally present in this system of equations and therefore 3-level leapfrog integrations of them will suffer from the instability described in Sec. II.

The set of constraint equations is comprised of the Hamiltonian constraint:

$$R - K_{ij}K^{ij} + K^2 = 0, \tag{19}$$

where $R = R_i^i$, and momentum constraints:

$$D_j(K^{ij} - g^{ij}K) = 0. \tag{20}$$

When the field variables and coordinate conditions for the spacetime are functions of time only, the Einstein equations [Eqs. (17) and (18)] governing the evolution of vacuum spacetimes become ordinary differential equations:

$$\frac{dg_{ij}}{dt} = -2\alpha K_{ij}, \tag{21}$$

$$\frac{dK_{ij}}{dt} = \alpha(KK_{ij} - 2K_{il}K_j^l). \tag{22}$$

This simplified set of equations is the basis of the toy codes discussed in Sec. VI A.

V. GOWDY T^3 SPACETIMES

In this section, we introduce the Gowdy T^3 spacetimes and then describe three classes of these spacetimes, for which exact evolution solutions are known and which we have used as relativistic testbeds for the deloused leapfrog technique (see Sec. VI).

The Gowdy T^3 spacetimes are solutions of the vacuum Einstein equations [Eqs. (17) and (18)] on the 3-torus, in which plane gravitational waves are contained within an expanding universe [30]. Solutions of Gowdy's equations have been used for studying the nature of the initial cosmological singularity [9,10], and, as is the case in this work, for testing numerical codes for solving Einstein's equations [31].

The Gowdy T^3 metric can be written:

$$ds^2 = e^{(\lambda-\tau)/2}(-e^{2\tau}d\tau^2 + dz^2) + e^\tau dw^2, \tag{23}$$

where

$$dw^2 = e^P(dx + Q dy)^2 + e^{-P}dy^2. \tag{24}$$

This form that appears in [10] is there attributed to Moncrief [32], whose exploitation of the harmonic map [33,34]

character of the associated Einstein equations could suggest many equivalent forms. The Gowdy coordinates τ , λ , σ , δ , and θ from [10] have here been written as $-\tau$, $-\lambda$, x , y , and z . The change in the signs of the time coordinate τ and of λ signify that time increases as the universe expands; in most earlier work, the emphasis on the study of the initial singularity dictated a time coordinate that increased as the universe contracted. The metric parameters λ , P , and Q are functions of z and τ only and are periodic in z .

We found the use of an alternate time variable

$$t = e^\tau \quad (25)$$

convenient in that it here makes the (coordinate) velocity of propagation of gravitational waves constant. This means that with a fixed spatial discretization size Δz the Courant condition will call for a fixed timestep Δt and thus makes the evolution easier to follow numerically. With this time coordinate, the Gowdy metric [Eq. (23)] becomes

$$ds^2 = t^{-1/2} e^{\lambda/2} (-dt^2 + dz^2) + t dw^2. \quad (26)$$

With an ingenious parameterization of the metric similar to Eq. (24), Gowdy found that the vacuum Einstein evolution equations could be written in terms of P and Q alone. With the metric in the form of Eq. (26), these become

$$P_{,tt} + t^{-1} P_t - P_{,zz} - e^{2P} (Q_{,t}^2 - Q_{,z}^2) = 0 \quad (27)$$

$$Q_{,tt} + t^{-1} Q_t - Q_{,zz} + 2(P_t Q_{,t} - P_{,z} Q_{,z}) = 0, \quad (28)$$

with the constraint equations specifying λ :

$$\lambda_{,z} = 2t(P_{,z} P_{,t} + e^{2P} Q_{,z} Q_{,t}) \quad (29)$$

$$\lambda_{,t} = t[P_{,t}^2 + P_{,z}^2 + e^{2P} (Q_{,t}^2 + Q_{,z}^2)]. \quad (30)$$

A. Kasner universe in power-law form

When the metric parameters P and Q are set to zero, the Gowdy metric [Eq. (26)] reduces to the simple diagonal form

$$ds^2 = t^{-1/2} e^{\lambda/2} (-dt^2 + dz^2) + t(dx^2 + dy^2). \quad (31)$$

This form of the metric represents a homogeneous, anisotropically expanding universe with no gravitational waves and is equivalent to the form of an axisymmetric Kasner metric [35] with a different time coordinate. A comparison of Eqs. (16) and (31) yields the following analytic solution for the time evolution of the diagonal components of the field variables ($g_{ij} = K_{ij} = 0$ for $i \neq j$) and coordinate conditions:

$$g_{11} = g_{22} = t \quad , \quad g_{33} = t^{-1/2} \quad , \quad (32)$$

$$K_{11} = K_{22} = -\frac{1}{2} t^{1/4} \quad , \quad K_{33} = \frac{1}{4} t^{-5/4} \quad , \quad (33)$$

$$\beta^i = 0 \quad , \quad (34)$$

$$\text{and} \quad \alpha = \sqrt{g_{33}} = t^{-1/4} \quad , \quad (35)$$

where we have used Eq. (17) to determine K_{ij} in terms of $g_{ij,t}$, β^i , and α , and have set λ , a constant in this case, to zero.

B. Kasner universe in exponential form

We can write the metric for the same Kasner universe with a different time coordinate in an exponential form

$$ds^2 = -e^t dt^2 + e^{2t/3} dx^2 + e^{2t/3} dy^2 + e^{-t/3} dz^2, \quad (36)$$

which is essentially the Gowdy metric given in Eq. (23) with $P = Q = \lambda = 0$. A comparison of Eqs. (36) and (16) gives the following analytic solution for $g_{ii}(t)$ and $K_{ii}(t)$ ($g_{ij} = K_{ij} = 0$ for $i \neq j$) and the coordinate conditions:

$$g_{11} = g_{22} = e^{2t/3} \quad , \quad g_{33} = e^{-t/3} \quad , \quad (37)$$

$$K_{11} = K_{22} = -\frac{1}{3} e^{t/6} \quad , \quad K_{33} = \frac{1}{6} e^{-5t/6}, \quad (38)$$

$$\beta^i = 0 \quad , \quad (39)$$

$$\text{and} \quad \alpha = \sqrt{g} = \sqrt{g_{11} \cdot g_{22} \cdot g_{33}} = e^{t/2} \quad , \quad (40)$$

where $g = \det(g_{ij})$ and we have once again used Eq. (17) to determine K_{ij} .

C. Polarized waves in an expanding universe

The Gowdy metric [Eq. (26)] with Q set to zero,

$$ds^2 = t^{-1/2} e^{\lambda/2} (-dt^2 + dz^2) + t(e^P dx^2 + e^{-P} dy^2), \quad (41)$$

represents the spacetime of an expanding universe containing polarized gravitational waves propagating in the z -direction. With this metric, the evolution equations [Eqs. (27) and (28)] reduce to a single linear equation for P :

$$P_{,tt} + t^{-1} P_t - P_{,zz} = 0. \quad (42)$$

The constraint equations become

$$\lambda_{,z} = 2t P_{,z} P_{,t} \quad (43)$$

and

$$\lambda_{,t} = t(P_{,t}^2 + P_{,z}^2). \quad (44)$$

The general solution to Eq. (42) is a sum of terms of the form $Z_0(2\pi n t) \cos(2\pi n z)$ and $Z_0(2\pi n t) \sin(2\pi n z)$,

where n is an integer (assuming periodicity of 1 in z) and Z_0 is a linear combination of the Bessel functions J_0 and Y_0 . We have chosen to study the spacetime based on the particular solution

$$P = J_0(2\pi t) \cos(2\pi z). \quad (45)$$

A comparison of the metrics given in Eqs. (16) and (41) then yields the following exact solution for the time evolution of the diagonal components of the field variables ($g_{ij} = K_{ij} = 0$ for $i \neq j$) and coordinate conditions:

$$g_{11} = te^P, \quad g_{22} = te^{-P}, \quad g_{33} = t^{-1/2}e^{\lambda/2}, \quad (46)$$

$$\begin{aligned} K_{11} &= -\frac{1}{2}t^{1/4}e^{-\lambda/4}e^P(1 + tP_{,t}), \\ K_{22} &= -\frac{1}{2}t^{1/4}e^{-\lambda/4}e^{-P}(1 - tP_{,t}), \\ K_{33} &= \frac{1}{4}t^{-1/4}e^{\lambda/4}(t^{-1} - \lambda_{,t}), \end{aligned} \quad (47)$$

$$\beta^i = 0, \quad (48)$$

and

$$\alpha = \sqrt{g_{33}} = t^{-1/4}e^{\lambda/4}, \quad (49)$$

where we have again used Eq. (17) to determine K_{ij} . This set of equations is completed by an expression for λ , which can be derived by using Eq. (45) in conjunction with Eqs. (43) and (44):

$$\begin{aligned} \lambda &= -2\pi t J_0(2\pi t) J_1(2\pi t) \cos^2(2\pi z) \\ &\quad + 2\pi^2 t^2 [J_0^2(2\pi t) + J_1^2(2\pi t)] \\ &\quad - \frac{1}{2} \{ (2\pi)^2 [J_0^2(2\pi) + J_1^2(2\pi)] - 2\pi J_0(2\pi) J_1(2\pi) \}. \end{aligned} \quad (50)$$

VI. NUMERICAL RELATIVITY SIMULATIONS

We have used the classes of Gowdy spacetimes discussed in Sec. V as testbeds for numerical relativity simulations using the deloused leapfrog, staggered leapfrog, and Crank-Nicholson time integration techniques discussed in Sec. II. We have carried out these simulations using two types of codes, toy codes (which solve the Einstein equations Eqs. (21) and (22) for spatially homogeneous spacetimes) and the ADM code developed by the Binary Black Hole (BBH) Grand Challenge Alliance [36,1] (which solves the full vacuum Einstein equations Eqs. (17) and (18) in three spatial dimensions). In this section, we present the results of these runs plus efficiency analyses that compare the numerical cost effectiveness of the various time integration schemes.

A. Toy code simulations

The vacuum Einstein equations for spatially homogeneous metrics reduce to the set of ordinary differential equations Eqs. (21) and (22). These are similar in form to the set of equations Eqs. (3), with the three-metric g_{ij} replacing \vec{r} and the extrinsic curvature K_{ij} replacing \vec{v} . Note that, as in the case of the full Einstein equations [Eqs. (17) and (18)], the system of Eqs. (21) and Eqs. (22) generally contains “velocity-dependent forces,” and thus 3-level leapfrog integrations of these equations will be inherently unstable. We have constructed toy codes to solve these equations using each of the integration methods discussed in Sec. II. The 3-level leapfrog toy code is based on the discretization in Eqs. (4), with the delousing module based on the Steps (1) - (5) outlined in Sec. III. The staggered leapfrog toy code is based on the discretization in Eqs. (11); in this method we use the extrapolation $K_{ij}^{n+1} = (3/2)K_{ij}^{n+1/2} - (1/2)K_{ij}^{n-1/2}$ to obtain K_{ij} on the full integer levels [37]. Although this extrapolation is accurate to second-order in Δt , it is not time symmetric. Finally, the Crank-Nicholson toy code is based on the discretization in Eqs. (12) - (14).

A toy code simulation of the Kasner universe in power-law form from Sec. V.A was the initial testbed numerical relativity problem to which we applied the deloused leapfrog technique. To demonstrate the need for the delousing modification of the standard 3-level leapfrog technique, we first carried out a run with the standard 3-level leapfrog technique itself. Eqs. (32)-(35) provide both the initial conditions for this simulation (begun at $t = 1$ and run with a timestep $\Delta t = 0.1$) and the means to measure its accuracy via a comparison between the analytically and numerically determined values of the field variables. Specifically, we use

$$e_g = \left[\sum_{i=1}^3 \left(\frac{g_{ii}}{g_{ii}^{an}} - 1 \right)^2 \right]^{1/2} \quad (51)$$

as a measure of a simulation’s accuracy. Here the analytic values of the diagonal components g_{ii} [given in this case by Eq. (32)] are denoted as g_{ii}^{an} . Another quantity useful in determining the quality of the integration is the size of the normalized residual of the vacuum Hamiltonian constraint [Eq. (19)]

$$H_{norm} = \frac{|R + K^2 - K_{ij}K^{ij}|}{|R| + K_i^j K_j^i}. \quad (52)$$

$R_i^i = R = 0$ for the spatially homogeneous Gowdy spacetimes. The results of the 3-level leapfrog simulation are presented in Fig. 3. Panels a and b of this figure display both the analytical (solid lines) and numerical (dots) solutions for the field variable components $g_{11}(t)$ and $K_{11}(t)$, respectively; panels c and d show the accuracy measures $H_{norm}(t)$ and $e_g(t)$, respectively. The separate

even and odd timestep numerical solutions, characteristic of the leapfrog instability described in Sec. II (cf. Eq. (8)), are clearly visible in all four panels of Fig. 3 as two dotted branches representing the numerical solution. The fact that these two dotted branches are indeed alternate timestep oscillations of the numerical solution is evident in the inset of Fig. 3a, which is an enlargement of the numerical solution of g_{11} for $37.9 < t < 39.2$. In this inset every value of g_{11} has been plotted with an “x” and consecutive values have been connected by dashed lines.

A toy code integration starting with the same initial conditions as the 3-level leapfrog run depicted in Fig. 3 was also performed with the deloused leapfrog technique. The trigger chosen to initiate the delousing steps in this run was a change in the sign of the slope of $H_{norm}(t)$; such a sign change is indicative of the alternate timestep oscillations discussed in the preceding paragraph. The results of this integration are given in Fig. 4. Panels a and b of this figure display the analytical (solid lines) and numerical (“x”s) solutions for $g_{11}(t)$ and $K_{11}(t)$, respectively; the solid lines in panels c and d represent $\log(H_{norm}(t))$ and $e_g(t)$, respectively. The regular behavior of the evolved quantities shown in Fig. 4 demonstrates that the delousing steps successfully removed the parasitic mode from the solutions for the field variables, producing an evolution that was stable for the duration of the integration. We ran the deloused code a factor of 25 times longer than the duration of the catastrophically unstable 3-level leapfrog simulation.

Note that in general it is possible to evolve components of g_{ij} or K_{ij} using the constraint equations [Eqs. (19-20)] in place of one or more of the evolution equations [Eqs. (17-18)]. For integrations of spatially homogeneous spacetimes, only the Hamiltonian constraint is meaningful in this context. In order to investigate the stability of such constrained evolutions, we performed 3-level leapfrog toy code simulations of the Kasner universe in exponential form in which we replaced the evolution equation for K_{33} [Eq. (22) with $i = j = 3$] with Eq. (19). Thus K_{33} was calculated in terms of the evolved quantities K_{11} and K_{22} by imposing the Hamiltonian constraint. These constrained runs still suffered from the instability under discussion. However, the times at which the simulations became catastrophically unstable were almost two and a half times longer than in the corresponding unconstrained runs.

We also carried out integrations of this model using the staggered leapfrog and Crank-Nicholson techniques. These runs were all stable, as expected.

Efficiency analysis of toy code runs

The efficiency of a stable integration technique is also an important factor to consider in evaluating numerical methods. Here, we consider the efficiency of a technique to be the accuracy level it maintains for a particular nu-

merical cost. Since the evaluation of the right-hand sides of the discretized equations [e.g., Eqs. (4), (11), and (14) for the set of equations Eqs. (3)] is generally the most expensive operation in terms of CPU time, we define the cost of an integration to be the number of times the right-hand sides are computed.

The results of our efficiency comparison for the toy code simulations of the Kasner universe in power-law form are displayed in Fig. 5. For this comparison, we ran simulations with each of the three stable integration methods; in these simulations the initial conditions and evolution duration were identical but the constant timestep used during the simulations Δt was varied from run to run. We used the value of e_g at the end of the simulation as the accuracy measure. The left panel of Fig. 5 gives the final values of $\log(e_g)$ as a function of $\log(\Delta t)$ and demonstrates that all three techniques are second-order accurate (i.e., the slope of $\log(e_g)$ versus $\log(\Delta t)$ for each method is ~ 2). The right panel of Fig. 5 gives the final values of $\log(e_g)$ as a function of the numerical cost (measured by the number of times both dg_{ij}/dt and dK_{ij}/dt are computed) and provides the most informative picture of the efficiency of the different techniques. The average number of iterations per timestep for the Crank-Nicholson runs ranged between two and three [for a convergence criterion of 1.0×10^{-8} ; see Sec. II]. The total number of delousing steps performed during the deloused leapfrog runs ranged from 153 to 181. Note that each delousing step adds eight calls to the cost of the integration since it requires four calls to the RK2 routine (see Sec. III), which in turn computes dg_{ij}/dt and dK_{ij}/dt twice. Panel b shows that, for simulations of this simple, spatially invariant spacetime, Crank-Nicholson is the most efficient of the three integrators. We have used least-squares analysis to fit the best straight lines to the data points shown in Fig. 5b. This analysis led to the following relationship for $e_g(\text{cost})$:

$$e_g = 10^{b_g} \text{cost}^{m_g}. \quad (53)$$

The values of the parameters b_g and m_g for these fits are given for each integrator in Table 1.

We have also done an efficiency comparison of these three integration techniques for toy code simulations of the Kasner universe in exponential form; the results are shown in Fig. 6. The outcome of the efficiency tests for these simulations is quite different from that based on the Kasner universe in power-law form of Fig. 5. Fig. 6b shows that for relatively low to moderate cost and accuracy demands, the staggered leapfrog method is the most cost effective technique in this case; however, the deloused leapfrog method is more efficient when high accuracy levels are required. The higher average number of iterations per timestep required by these Crank-Nicholson runs, which ranged from three for $\Delta t = 0.0016$ to seven for $\Delta t = 0.1$, may account for the reversal in its relative cost effectiveness from the simulations of the power-law form (Fig. 5). The number of delousing steps

taken during the deloused leapfrog runs ranged from 1285 for $\Delta t = 0.0016$ to 422 for $\Delta t = 0.1$. Thus the deloused leapfrog method had to work harder to maintain stable integrations of this universe in exponential form than in power-law form. We have again used least squares analysis to fit straight lines to the data in Fig. 6b and produce a relation of the form of Eq. (53); this relation is parameterized by the values of b_g and m_g given in Table 2.

B. ADM code simulations

Our study of the deloused leapfrog method stems from our search for an efficient technique capable of performing numerically stable simulations of the orbital dynamics of binary neutron stars. Because such simulations require the solution of the full Einstein equations, we wanted to test the deloused leapfrog integrator in conjunction with the code we plan to use to do these simulations, the ADM code developed by the BBH Alliance [36,1]. This second-order accurate code currently solves the vacuum Einstein equations on a Cartesian grid and provides the user the choice of utilizing either the standard 3-level leapfrog or Crank-Nicholson integration techniques. We have added the capability of using the deloused leapfrog integrator to the BBH Alliance’s ADM code and have used it to perform simulations of a Kasner (homogeneous Gowdy) expanding spacetime with the power-law coordinate condition of Sec. V.A and of the expanding Gowdy spacetime with polarized gravitational waves of Sec. V.C. Of course this code, like the toy code, was ignorant of Gowdy’s ingenuity which, through parameterizations like $g_{11} = t e^P$, can reduce some of the Einstein equations to linear equations. The Einstein equations are coded in terms of the g_{ij} and K_{ij} as shown in Eqs. (17) and (18); the chosen coordinate conditions were $\beta^i = 0$ and $\alpha = \sqrt{g_{33}}$. They involve not only the polynomial nonlinearities manifest in these equations, but also the nonlinearities implied through α and through the inverse metric when indices are raised or covariant derivatives or curvatures are computed.

The preliminary testbed used in our ADM code runs was a simulation identical to the toy code runs of the Kasner power-law metric. The development of the instability in the ADM code’s 3-level leapfrog run replicated its development in the toy code run. The ADM code’s deloused leapfrog run successfully removed this instability in the same manner as in the toy code run, with the delousing steps triggered at the same temporal intervals in both simulations.

To test the behavior of the deloused leapfrog method for partial differential equations with spatially varying terms, we carried out simulations of the polarized Gowdy spacetime of Sec. V.B. Equations (45)-(30) yield both initial conditions for simulations of this spacetime and exact solutions with which to compare the results of such

simulations.

Our ADM code polarized Gowdy simulations began at $t = 1$ and were run with periodic boundary conditions over the interval $-\frac{1}{2} \leq z \leq \frac{1}{2}$ and a grid spacing $\Delta z = 1/62$. Because the vacuum Einstein equations are partial differential equations, the size of the timestep that can be taken in the integration is restricted by the Courant condition [25], which ensures that information cannot propagate across more than a single grid zone in one timestep. For the polarized Gowdy metric of Eq. (41), this condition is equivalent to enforcing $\Delta t = C \Delta z$, where Δz is the (uniform) grid spacing and the Courant factor $C < 1$. In the runs presented here, we chose $C = 0.3$. The initial ADM code simulation was performed with the 3-level leapfrog integrator and, as expected, was unstable. The results of the integration are presented in Figs. 7 and 8. The evolution of the value of g_{11} at the center of the grid is shown in panel a of Fig. 7; panels b, c, and d of this figure display, respectively, $\overline{H}_{norm}(t)$, $\overline{e}_g(t)$, and $\overline{e}_t(t)$. Here bars denote (spatial) averages over the grid. $\overline{H}_{norm}(t)$ is computed by dividing the spatial average of the numerator of Eq. (52) by the spatial average of the denominator of Eq. (52). The additional measure of the accuracy of the simulation, e_t , is defined by

$$e_t(x, y, t) = t^{-1} |t - [g_{11}(x, y, x) g_{22}(x, y, x)]^{1/2}|. \quad (54)$$

The usefulness of e_t as an error estimate arises because, according to the analytic solution of Eq. (46), $g_{11} g_{22} = t^2$.

The separate even and odd timestep solutions, indicative of the instability, can clearly be seen in the plots of $\overline{H}_{norm}(t)$, $\overline{e}_g(t)$, and $\overline{e}_t(t)$; however, the separate solutions are not yet visible in the plot of g_{11} at $t = 5.8$. As shown in Fig. 8, they do appear in g_{11} at the grid center later in the evolution, as the instability begins to overwhelm the computation.

We then evolved the same polarized Gowdy initial data with the ADM code using the deloused leapfrog integrator. Because $\overline{H}_{norm}(t)$ and $\overline{e}_g(t)$ oscillated in our simulations of this spacetime, they were not used as a basis for the trigger that initiated the delousing steps. [These fluctuations are due to the complex oscillatory nature of g_{ij} and K_{ij} in this spacetime and are *not* related to the alternate timestep oscillations caused by the instability; in fact, such fluctuations are also present in the Crank-Nicholson simulations of this spacetime.] Instead, because \overline{e}_t behaved monotonically (see Fig. 9d), a change in the sign of its temporal slope was used as the delousing trigger. As can be seen in Fig. 9, the removal of the parasitic mode during the delousing steps taken in this simulation eliminated the presence of large alternate timestep oscillations and allowed for a stable integration.

Efficiency analysis of ADM code runs

We have also used simulations of this polarized Gowdy spacetime to evaluate the efficiency of the deloused

leapfrog algorithm. However, in this case its performance could only be compared with that of the Crank-Nicholson technique, as the staggered leapfrog method has not been implemented in the ADM code. (The reason for this is that the memory requirements of the staggered leapfrog method would exceed those of the other two methods if adaptive mesh refinement were to be used.) In this efficiency comparison, Δz and Δt are reduced in tandem from run to run, with C held constant at 0.3. The value of \bar{e}_t at the end of the simulations was used as the measure of accuracy upon which to base the efficiency analysis in this case.

The results of this analysis are displayed in Fig. 10. The left panel of this figure gives the final value of \bar{e}_t as a function of the grid spacing Δz , which was varied from 1/126 to 1/62 to 1/30. Straight lines fit through these data points have slopes ~ 2 ; this demonstrates the second-order accuracy of the deloused leapfrog and Crank-Nicholson methods. The right panel contains a plot of \bar{e}_t versus cost and indicates that the deloused leapfrog integrations of this spacetime were about five to eight times more efficient than those carried out with the Crank-Nicholson technique. The average number of iterations per timestep for the Crank-Nicholson runs ranged from five for $\Delta z = 1/126$ to eight for $\Delta z = 1/30$. The total number of delousing steps taken was relatively constant in the three deloused leapfrog runs (six for $\Delta z = 1/126$; five for $\Delta z = 1/62$; and six for $\Delta z = 1/30$). The least squares straight line fits to the data in Fig. 10b can be transformed, in this case, to relations of the form

$$e_t = 10^{b_t} \text{cost}^{m_t}; \quad (55)$$

the parameters b_t and m_t determined by these fits are given in Table 3.

VII. CONCLUSIONS

The purpose of this paper is to alert the community to the existence of the instability inherent in standard 3-level leapfrog integrations of Einstein's equations and to demonstrate that the proposed delousing modification to the standard algorithm can efficiently cure this instability. To this end, we have used three classes of testbed solutions. In Sec. III, we show calculations of highly relativistic circular geodesic orbits calculated in Cartesian coordinates. In Sec. VI, we show evolutions of homogeneous expanding cosmologies and polarized gravitational waves in an expanding Gowdy spacetime. In all of these cases, the deloused leapfrog algorithm removed parasitic modes from the numerical solution of the Einstein equations that were excited to instability in traditional 3-level leapfrog simulations of these spacetimes, and thus allowed for their stable evolution.

The numerical efficiency (i.e., the accuracy level maintained for a particular numerical cost) of the deloused leapfrog integrator was compared to the efficiencies of

two other stable integration methods, staggered leapfrog and Crank-Nicholson. We have defined numerical cost as the number of times the right hand sides of both Einstein evolution equations (i.e., $g_{ij,t}$ and $K_{ij,t}$) are computed during a simulation. Thus cost in this case is a measure of a simulation's CPU expense. Note that all of the simulations presented in this paper were carried out with constant timesteps.

The first testbed for this efficiency analysis was a toy code (which solves the spatially invariant Einstein equations [Eqs. (21) and ((22))] simulation of a spatially homogeneous Gowdy spacetime yielding a Kasner universe. With the coordinate condition choice $\alpha = \sqrt{g_{33}}$ this gives a power-law analytic solution for the metric components. For this simple problem, Crank-Nicholson was the most efficient of the integrators (see Fig. 5). The results were different, however, when the testbed was changed to a toy code simulation of the same Kasner universe with a different time coordinate choice $\alpha = \sqrt{g} = \sqrt{g_{11} \cdot g_{22} \cdot g_{33}}$, yielding in the analytic solution an *exponential* form for the metric components. In that case, the staggered and deloused leapfrog techniques were more cost effective (see Fig. 6), as the rapid evolution of the spacetime caused the iterative Crank-Nicholson technique to require a larger number of iterations per timestep.

The final testbed used in our efficiency analysis was a simulation of an expanding Gowdy spacetime containing polarized gravitational waves. These simulations required the solution of the complete vacuum Einstein equations and were carried out with the BBH Alliance's ADM code [36,1], in which the standard (unstable) 3-level leapfrog and the (stable) Crank-Nicholson integration methods had previously been implemented. We modified this code to allow the use of the deloused leapfrog scheme. Because the staggered leapfrog method has not been implemented in the ADM code, the efficiencies of only the Crank-Nicholson and deloused leapfrog integrators were evaluated in this case. The deloused leapfrog integrations of this spacetime were five to eight times more cost effective than the Crank-Nicholson runs (see Fig. 10).

Thus, the results of our testbed simulations indicate that the deloused leapfrog algorithm is an effective and efficient cure for the 3-level leapfrog instability. Further evaluation of this algorithm, via its use in more complex problems in numerical relativity, such as a contracting Gowdy universe containing unpolarized gravitational waves, and other fields, would serve to confirm the robustness of the method and provide insight into its cost effectiveness in different numerical scenarios.

One aspect of the deloused leapfrog algorithm that has the potential to alter the conclusions of such efficiency analyses is the choice of delousing trigger. Based on our experience, we suspect that choice of a trigger which initiates an *excessive* number of delousing steps will degrade the accuracy of a simulation to some degree. If this is the case, a decrease in the average interval between delousing steps would not only increase the cost of the run, but

would also decrease its numerical accuracy somewhat. On the other hand, an increase in the delousing interval would allow the parasitic mode in the numerical solution to grow to higher levels. For example, had a change in the sign of the temporal slope of $g_{11}(t)$ been used as the delousing trigger in the deloused leapfrog simulation of the polarized Gowdy spacetime, the parasitic mode would likely have grown to a greater extent between delousing intervals, as its presence became sizeable in $g_{11}(t)$ rather late in the evolution (see Figs. 7 and 8). Thus the choice of delousing trigger may involve a trade-off between the loss of some degree of accuracy introduced into the computation via the delousing steps and the degree to which the parasitic mode is permitted to grow between these steps.

In conclusion, we have demonstrated that the deloused leapfrog algorithm permits the stable numerical evolution of simple vacuum spacetimes. In addition, our results suggest that deloused leapfrog may be a better integration technique than Crank-Nicholson to employ in complex numerical relativity simulations, as this new algorithm was more cost effective than the Crank-Nicholson method in our simulation of a spatially varying spacetime.

ACKNOWLEDGMENTS

We thank Matt Choptuik, Alex Dragt, Mijan Huq, Scott Klasky, Steve McMillan, and Conrad Schiff for interesting and helpful discussions. We are grateful to the Binary Black Hole Alliance (NSF ASC/PHY 938152-ARPA Supplemented, R. Matzner PI) for making their ADM code available to us, and to Mijan Huq and Scott Klasky for helping us to learn how to run the code. We also thank the anonymous referee for thoughtful comments that resulted in improvements in this manuscript.

This work was supported in part by NSF grants PHY 9208914 and PHY 9722109 at Drexel, and PHY 9700672 at the University of Maryland. The numerical simulations using the ADM code were run at the Northeast Parallel Architectures Center (NPAC) at Syracuse University.

[1] A. M. Abrahams *et al.*, Phys. Rev. Lett. (submitted; gr-qc/9709082); G. B. Cook *et al.*, Phys. Rev. Lett. (submitted; gr-qc/9711078).
 [2] G. J. Mathews and J. R. Wilson, *Astrophys. J.* **482**, 929 (1997).
 [3] T. Piran and R. Stark, in *Dynamical Spacetimes and Numerical Relativity*, edited by J. Centrella (Cambridge University Press, New York, 1986).
 [4] A. Abramovici *et al.*, *Science* **256**, 325 (1992).

[5] C. Bradaschia *et al.*, *Nucl. Instrum. & Methods* **A289**, 518 (1990).
 [6] K. Danzmann *et al.*, in *Relativistic Gravity Research*, Proceedings of the 81WE-Heraus-Seminar, Bad Hannef, Germany, edited by J. Ehlers and G. Schäfer (Springer-Verlag, Berlin, 1992); J. Hough *et al.*, Proposal for a 600 m Laser-Interferometric Gravitational Wave Antenna, 1994 (unpublished).
 [7] P. Anninos *et al.*, *Phys. Rev. D* **56**, 842 (1997); M. Shibata and T. Nakamura, *Phys. Rev. D* **52**, 5428 (1995); P. Anninos, J. Centrella, and R. Matzner, *Phys. Rev. D* **43**, 1825 (1991); **39**, 2155 (1989); T. Nakamura *et al.*, *Prog. Theor. Phys. Suppl.* **90**, 1 (1987); *Prog. Theor. Phys.* **65**, 894 (1981).
 [8] H. Kurki-Suonio and J. Centrella, *Phys. Rev. D* **43**, 1087 (1991).
 [9] B. Grubišić and V. Moncrief, *Phys. Rev. D* **47**, 2371 (1993).
 [10] B. Berger and V. Moncrief, *Phys. Rev. D* **48**, 4676 (1993).
 [11] M. W. Choptuik, *Phys. Rev. Lett.* **70**, 9 (1993); in *Deterministic Chaos in General Relativity*, edited by D. Hobill *et al.* (Plenum, New York, 1994), p. 155; A. Abrahams and C. Evans, *Phys. Rev. Lett.* **70**, 2980 (1993).
 [12] R. D. Ruth, *IEEE Transactions on Nuclear Science* **NS-30**, 2669–71 (1983); E. Forest and R. D. Ruth, *Physica D* **43**, 105–117 (1990).
 [13] P. Hut, J. Makino, and S. McMillan, *Astrophys. J. Lett.* **443**, 93 (1995).
 [14] T. Quinn *et al.*, *Astrophys. J.* (submitted; astro-ph/9710043).
 [15] N. A. Phillips in *The Atmosphere and the Sea in Motion*, B. Bolin ed., Rockefeller Institute, New York, 1959, pp. 501–504.
 [16] B. Fornberg, *Maths. of Computation*, **27**, 45–57 (1973).
 [17] J. M. Sanz-Serna, *SIAM J. Sci. Statist. Comput.* **6**, 923–938 (1985).
 [18] A. Aoyagi and K. Abe, *J. Comp. Phys.* **83**, 447 (1989).
 [19] D. Cai, A. Aoyagi, and K. Abe, *J. Comp. Phys.* **107**, 146–151 (1993).
 [20] J. M. Sanz-Serna and F. Vasilillo, *SIAM J. Appl. Math.* **47**, 92–108 (1987).
 [21] K. Watt and C. W. Misner, (in preparation).
 [22] A. Aoyagi and K. Abe, *J. Comp. Phys.* **93**, 287 (1991).
 [23] F. Vasilillo and J. M. Sanz-Serna, *J. Comp. Phys.* **66**, 225 (1986).
 [24] L. D. Landau and E. M. Lifshitz, *Mechanics*, (Pergamon Press, Oxford, 1960, 1969, 1976), §27; N. W. McLachlan, *Theory and Applications of Mathieu Functions*, (Dover, 1964 reprint, Oxford University Press, 1947), Chapter 1; for more recent work see, e.g., W. E. Wiesel and D. J. Pohlen, *Celest. Mech. and Dynam. Astron.* **58**, 81–96 (1994).
 [25] W. H. Press *et al.*, *Numerical Recipes* (Cambridge University Press, Cambridge, 1989), p. 627.
 [26] B. Gustafsson, H-O. Kreiss, and J. Olinger, *Time Dependent Problems and Difference Methods* (Wiley, New York, 1995).
 [27] C. Misner, K. Thorne, and J. Wheeler *Gravitation* (Freeman, New York, 1973).
 [28] R. Arnowitt, S. Deser, and C. W. Misner, Chapter 7 in

Gravitation: An Introduction to Current Research edited by L. Witten (Wiley, New York, 1962), pp. 227-265.

- [29] E. Seidel, in *Relativity and Scientific Computing*, edited by F. Hehl, R. Puntigam, and H. Ruder (Springer, New York, 1996), p. 25.
- [30] R. H. Gowdy, *Phys. Rev. Lett.* **27**, 826 (1971); *Ann. Phys. (N.Y.)* **83**, 203 (1974).
- [31] M. H. P. M. van Putten, *Phys. Rev. D* **55**, 4705 (1997).
- [32] V. Moncrief, *Ann. Phys. N.Y.* **132**, 87–107 (1981).
- [33] J. Eells and J. Samson, *Amer. J. Math.* **78**, 109 (1964).
- [34] C. Misner, *Phys. Rev. D* **18**, 4510 (1978).
- [35] E. Kasner, *Am. J. Math.* **43**, 217 (1921).
- [36] The Binary Black Hole Grand Challenge Alliance, <http://www.npac.syr.edu/projects/bh>.
- [37] P. Anninos, *Phys. Rev. D* **52**, 2059 (1995).

FIG. 1. The numerical integration of the geodesic equations for a particle in the Schwarzschild spacetime using the 3-level leapfrog technique. The geodesic equation was solved in rectangular coordinates from a 3D Hamiltonian (see [21]). The particle was given initial conditions such that it should remain on a circular orbit of radius $r_0 = 10M$ and have an orbit period of $199M$. In each frame, the data is plotted on every twenty-third timestep ($\Delta t = 0.1M$). The instability manifests as the solutions on odd (circles) and even (triangles) timesteps diverge. Although the integrator appears to be stable at early times, the parasitic mode is present from the beginning, on a much smaller scale than is used in these plots. The integrator failed and the code crashed after ~ 6 orbital periods. (a) The particle orbit in the x - y plane. (b) The magnitude of the particle’s position vector as a function of time.

FIG. 2. Same as Fig. 1 except that the integration was carried out using the deloused leapfrog method. The orbit is now stable for the $\sim 10,000$ -orbit duration of the simulation. The timestep was the same as that used in Fig. 1, but the data is plotted only every 2001 timesteps. Note that even though only ~ 1 point per orbit (each orbit is approximately 2000 timesteps) are shown, there are over 10,000 points plotted in the figure. Both odd and even solutions lie directly on top of each other, filling out the orbit track. The delousing module was applied on average once every 405 timesteps, hence this figure was produced at a 2 percent increase in CPU cost per orbit over the simulation shown in Fig. 1.

FIG. 3. The results of the unstable 3-level leapfrog toy code integration of a Kasner universe in power-law form are presented here. The numerical (dots, with every other pair of even and odd timestep values plotted) and analytical (solid lines) solutions for $g_{11}(t)$ and $K_{11}(t)$ are given in panels a and b, respectively. The inset in panel a is an enlargement of the numerical solution for $g_{11}(t)$ in the range $37.9 < t < 39.2$, in which all data points have been plotted and connected with dashed lines to emphasize the large alternate timestep oscillations of this unstable solution. The numerical accuracy measures $H_{norm}(t)$ and $e_g(t)$ are shown in panels c and d, respectively; for the sake of clarity, only every other pair of even and odd timestep values has been plotted.

FIG. 4. This figure depicts the stable deloused leapfrog, toy code integration begun with the same initial conditions as the unstable 3-level leapfrog simulation presented in Fig. 3. The numerical (“x”s, with every 201st point plotted) and analytical (solid line) solutions for $g_{11}(t)$ and $K_{11}(t)$ are given in panels a and b, respectively. The accuracy measures $\log(H_{norm}(t))$ and $e_g(t)$ are shown in the lower panels c and d, respectively.

FIG. 5. The results of the efficiency analysis of toy code simulations of a Kasner universe in power-law form, represented by the metric given in Eq. (31), carried out with different integration techniques are shown here. The final values of $\log(e_g)$ are plotted versus $\log(\Delta t)$ in the left panel and versus $\log(\text{cost})$ in the right panel. Values from Crank-Nicholson runs are marked with “x”s, those from deloused leapfrog runs are marked with triangles, and those from staggered leapfrog runs are marked with squares. The cost is defined as the number of times the right-hand sides of the discretized equations are evaluated. The slopes of straight lines fit through data in (a) are ~ 2 , indicating that the numerical techniques are all accurate to second-order in Δt .

FIG. 6. The same quantities and notation as in Fig. 5, but for toy code simulations of a Kasner universe in exponential form, described by the metric of Eq. (36).

FIG. 7. The results of the unstable 3-level leapfrog ADM code integration of the expanding universe containing polarized gravitational waves are presented here. The numerical (dots, with every fourth pair of even and odd timestep data points plotted) and analytical (solid line) solutions for $g_{11}(t)$ at the grid center are given in panel a. The numerical accuracy measures \overline{H}_{norm} , \overline{e}_g , and \overline{e}_t are plotted as functions of time in panels b, c, and d, respectively; again, only every fourth pair of even and odd timestep values has been plotted.

FIG. 8. The extended evolution of the metric component g_{11} , at the grid center, from the unstable 3-level leapfrog simulation presented in Fig. 7 is shown here. The notation is the same as that of panel a in Fig. 7 (except that every other pair of even and odd timestep values is plotted), but the duration of the evolution has been extended to exhibit the growth of the parasitic mode, as evidenced by the appearance of the even and odd timestep branches of the numerical solution.

FIG. 9. This figure depicts the stable deloused leapfrog, ADM code integration begun with the same initial conditions as the unstable 3-level leapfrog simulations shown in Figs. 7 and 8. The numerical (“x”s, with every eleventh point plotted) and analytical (solid line) solutions for $g_{11}(t)$ at the center of the grid are given in panel a. Panels b, c, and d present the evolutions of the accuracy measures \overline{H}_{norm} , $\overline{\epsilon}_g$, and $\overline{\epsilon}_t$, respectively.

FIG. 10. The results of the efficiency analysis of ADM code simulations of an expanding universe containing polarized gravitational waves, represented by the metric of Eq. (41), are shown here. The final values of $\log(\overline{\epsilon}_t)$ are plotted as a function of the logarithm of the grid spacing Δz ($\Delta t = 0.3 \Delta z$) in the left panel and as a function of the logarithm of the numerical cost in the right panel. Triangles mark the data points from deloused leapfrog runs; “x”s mark those from Crank-Nicholson runs. Straight lines fit through data points in the left panel have slope ~ 2 , indicating that the numerical techniques are both accurate to second-order in Δt .

TABLE I. Parameters for fits to accuracy versus cost data in Fig. 5

Method	b_g	m_g
deloused leapfrog	6.6	-2.0
Crank-Nicholson	6.8	-2.2
staggered leapfrog	6.7	-2.0

TABLE II. Parameters for fits to accuracy versus cost data in Fig. 6

Method	b_g	m_g
deloused leapfrog	11	-3.1
Crank-Nicholson	9.0	-2.6
staggered leapfrog	5.8	-1.9

TABLE III. Parameters for fits to accuracy versus cost data in Fig. 10

Method	b_t	m_t
deloused leapfrog	4.8	-2.1
Crank-Nicholson	9.6	-2.8

Figure 1

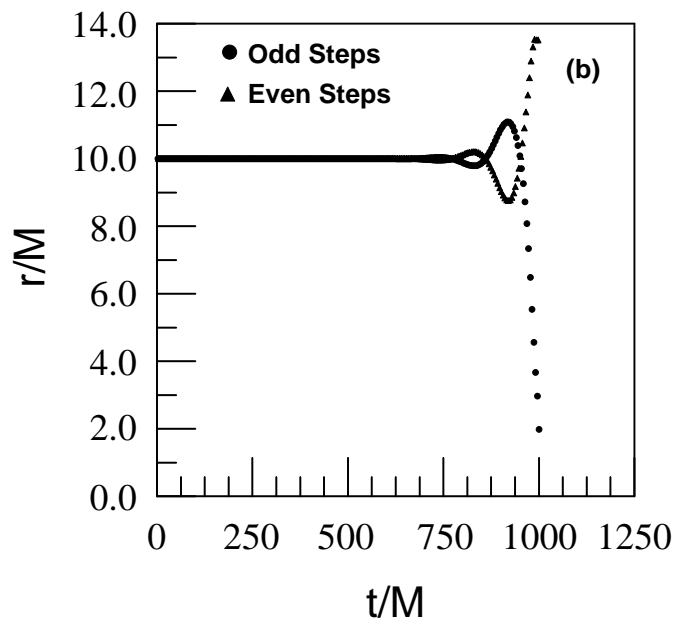
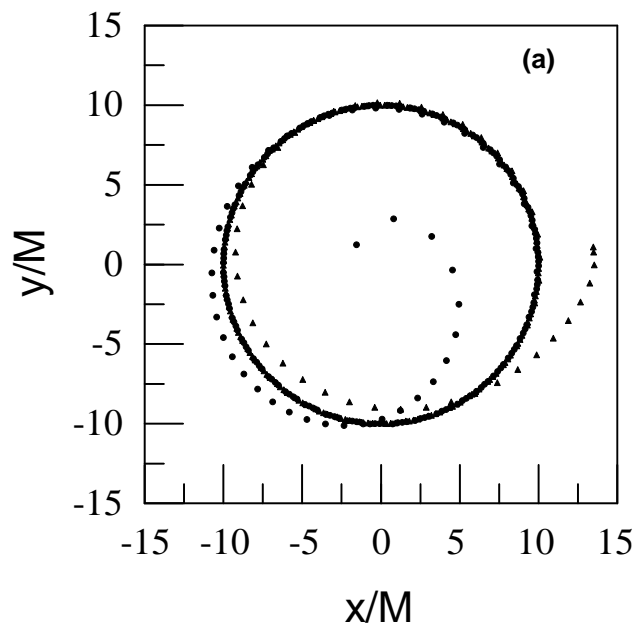


Figure 2

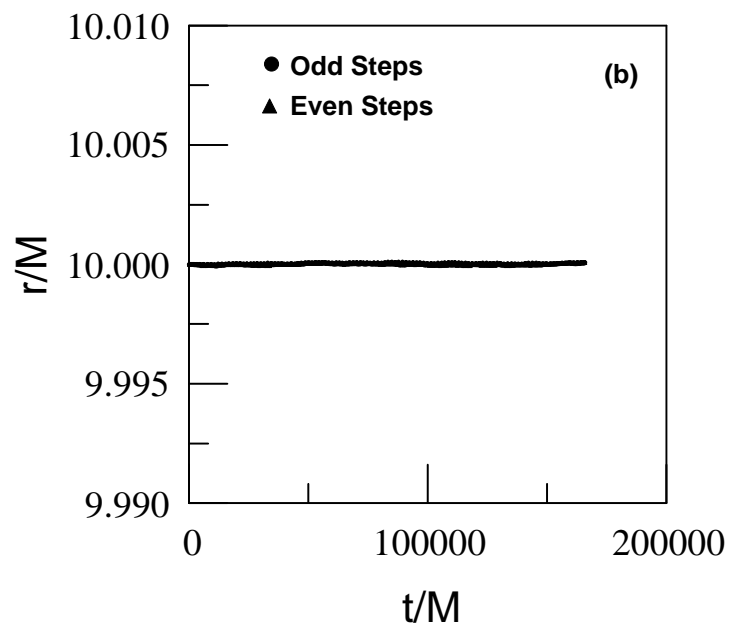
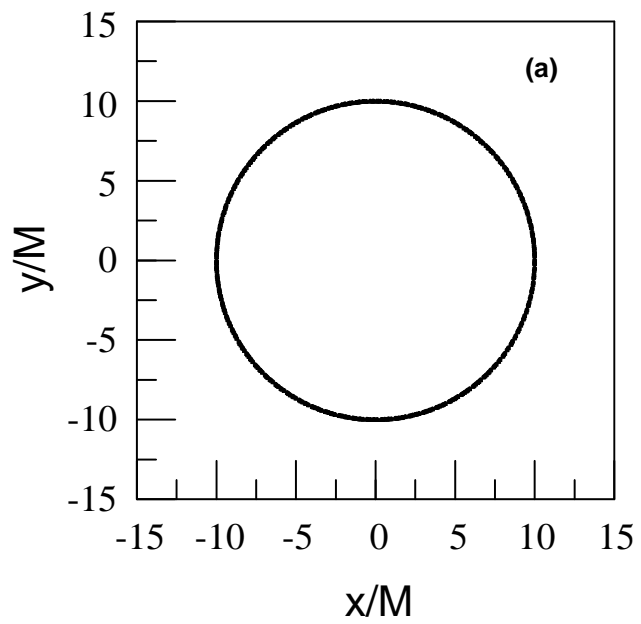


Figure 3

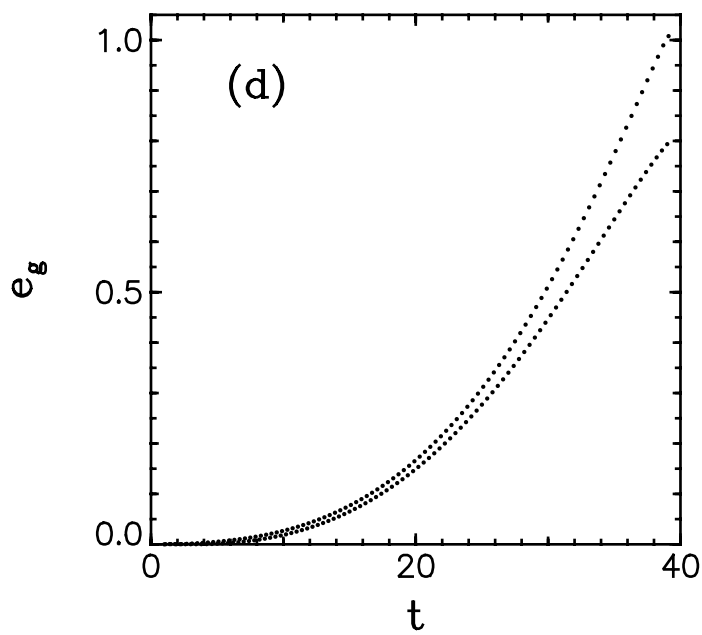
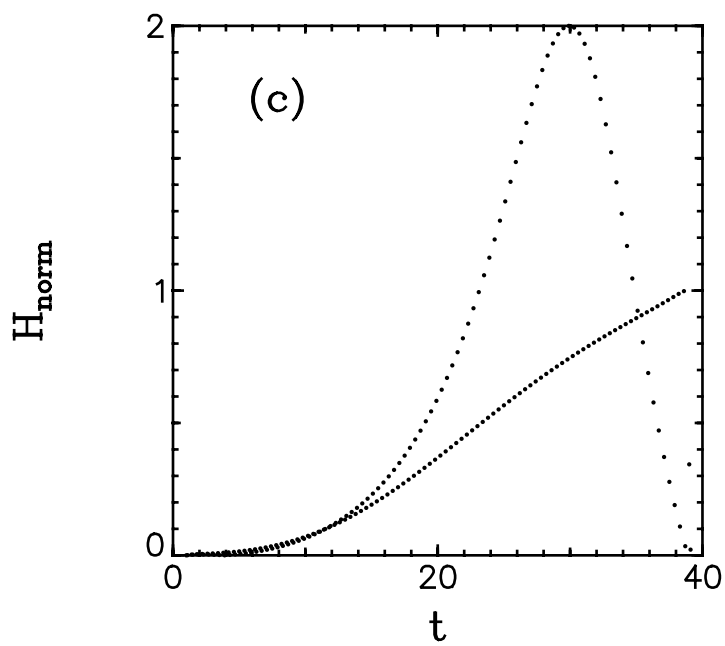
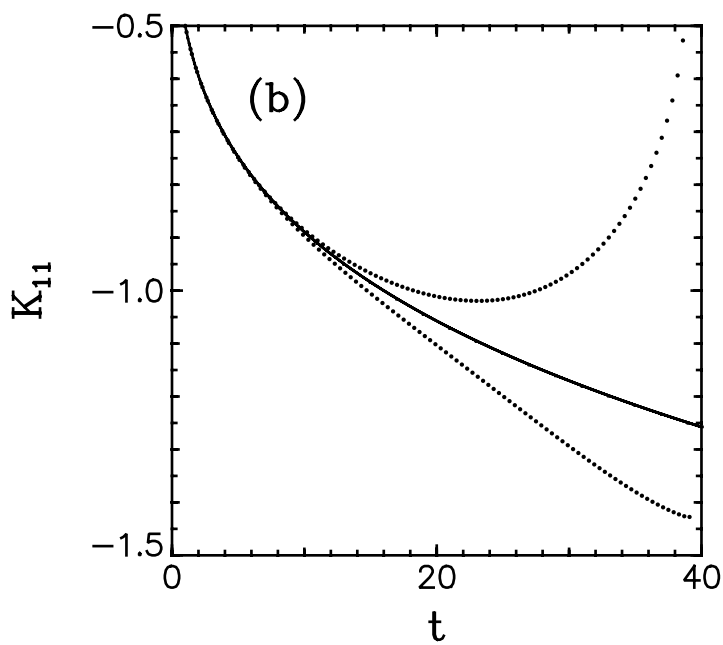
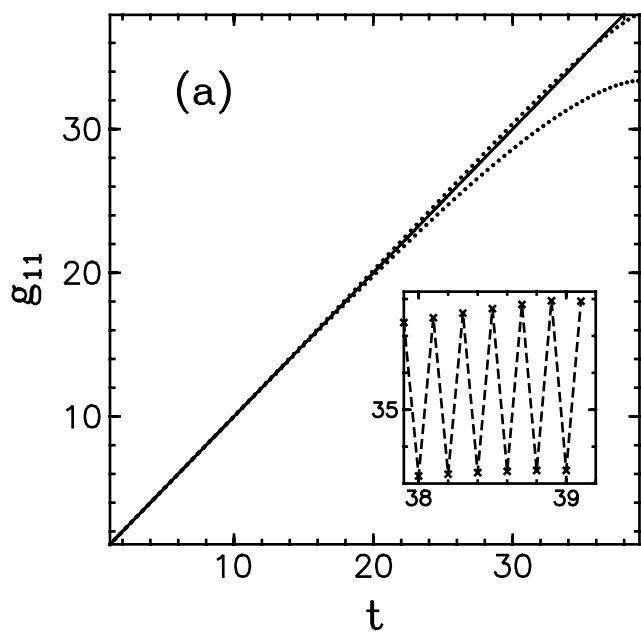


Figure 4

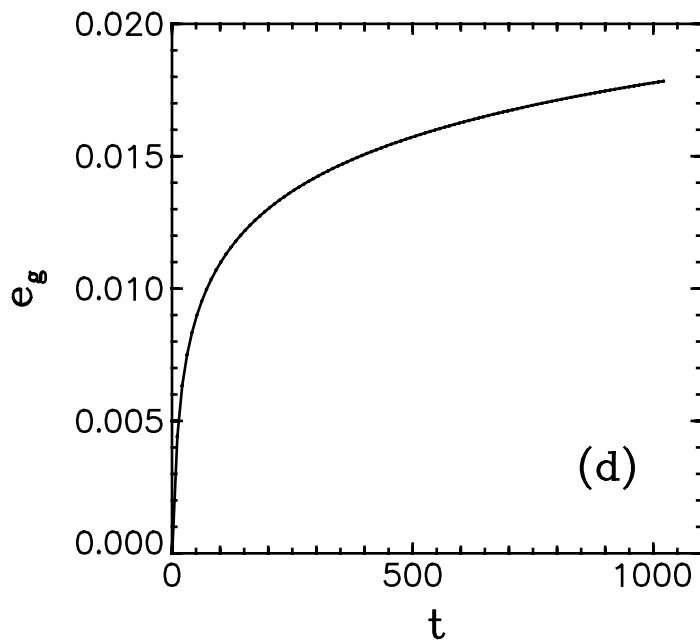
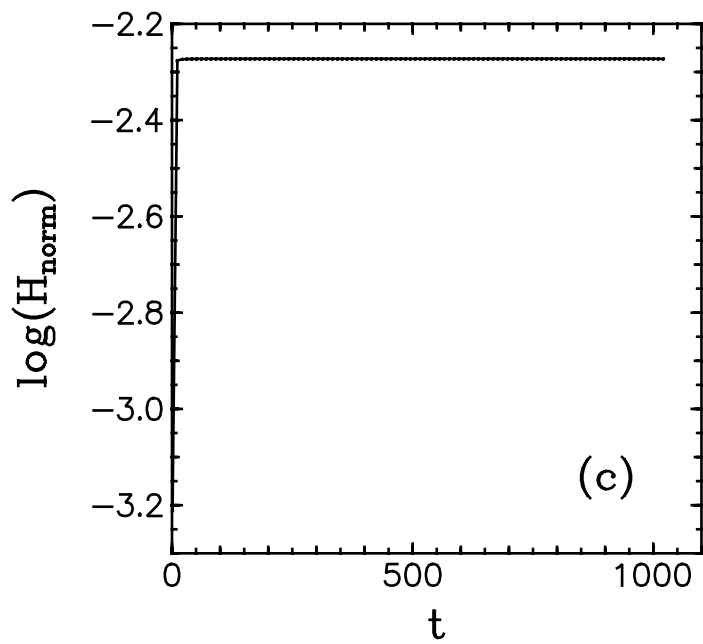
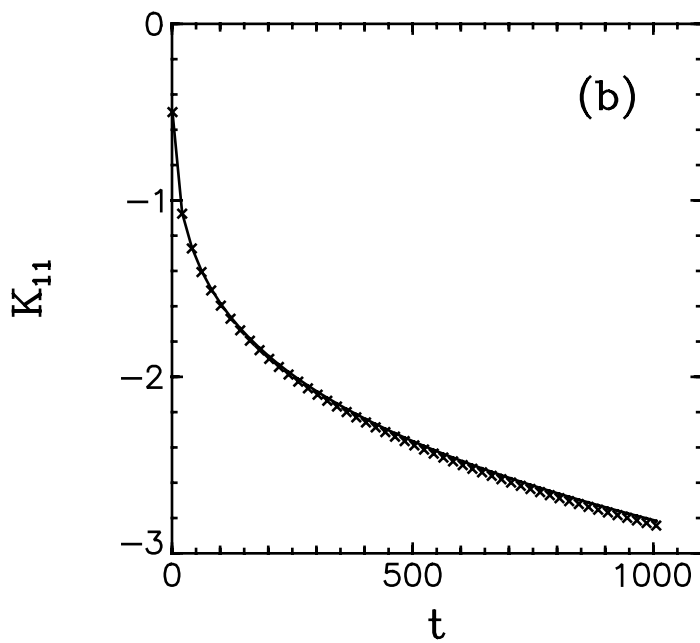
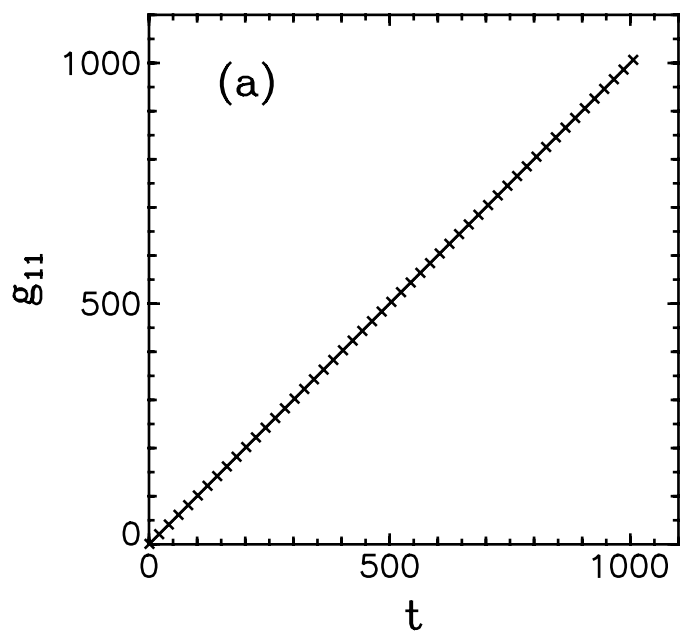


Figure 5

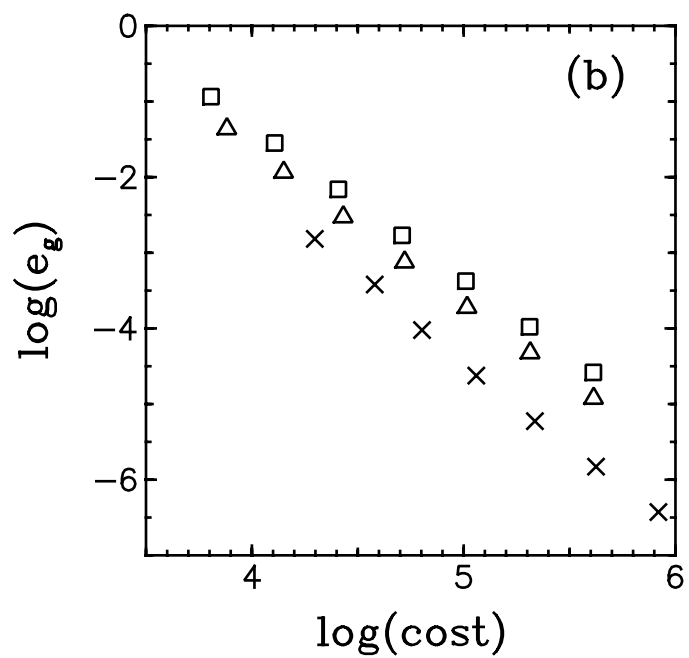
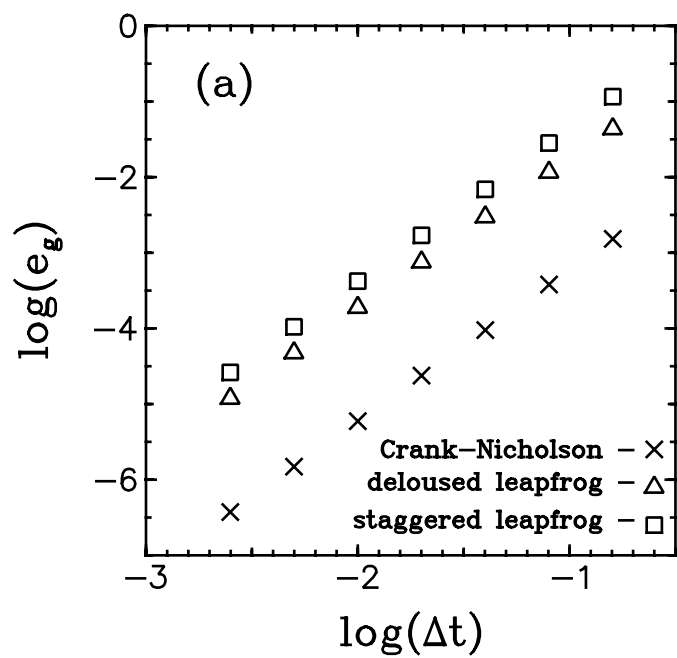


Figure 6

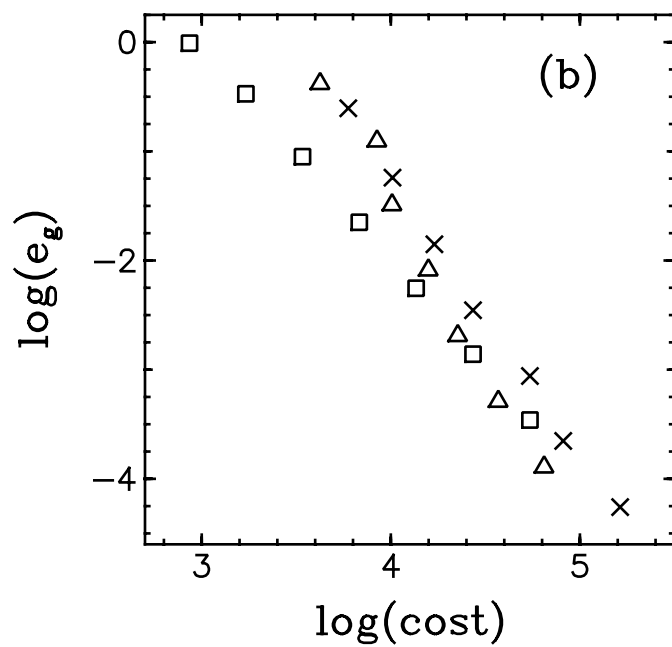
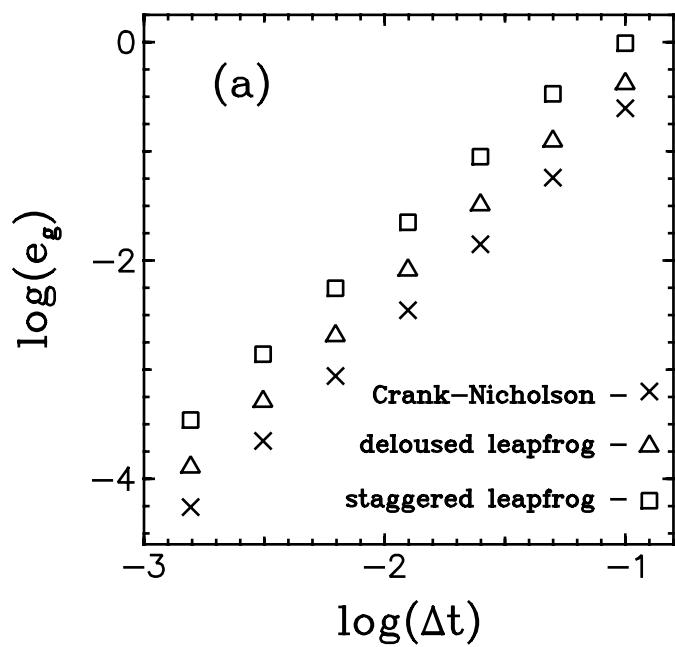


Figure 7

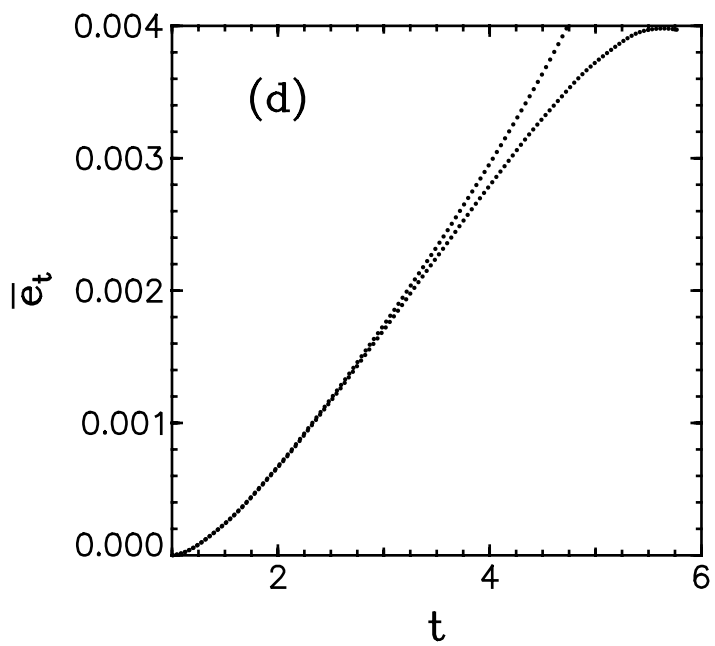
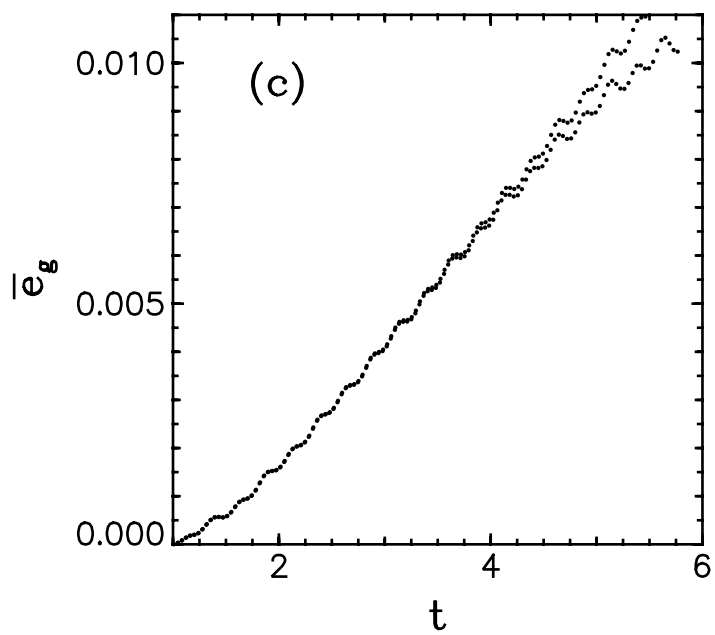
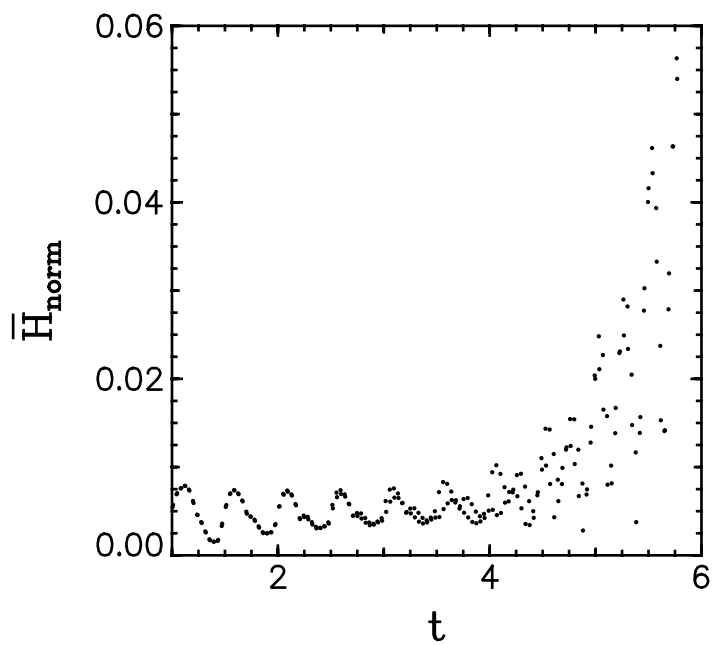
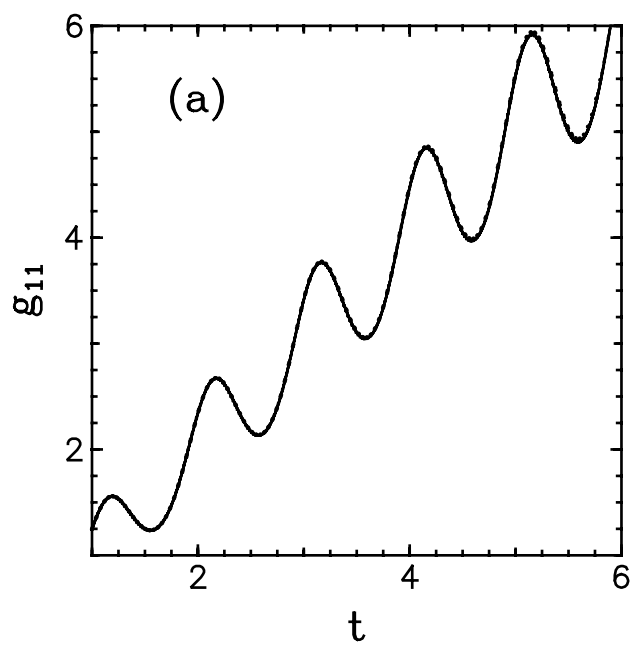


Figure 8

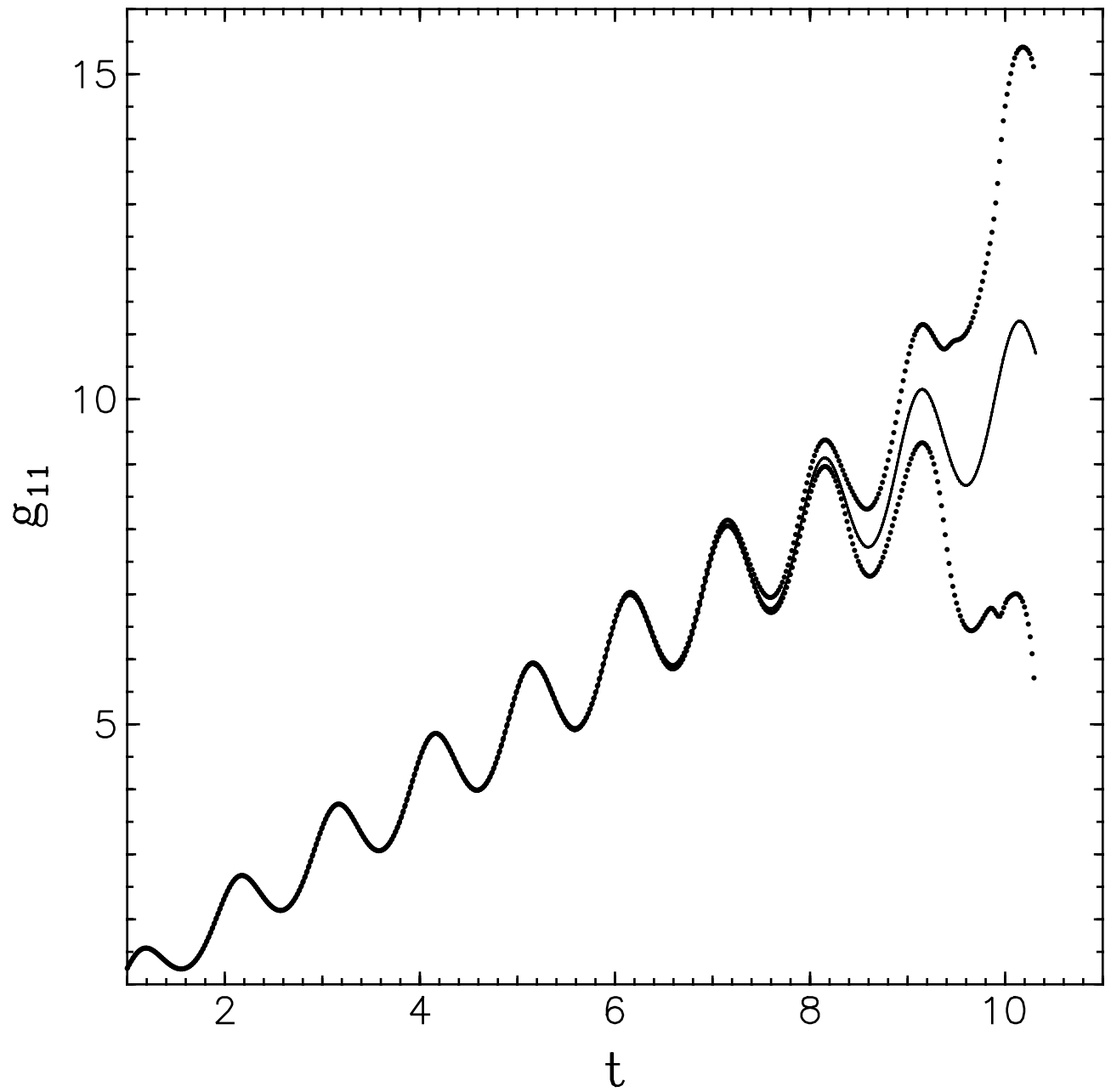


Figure 9

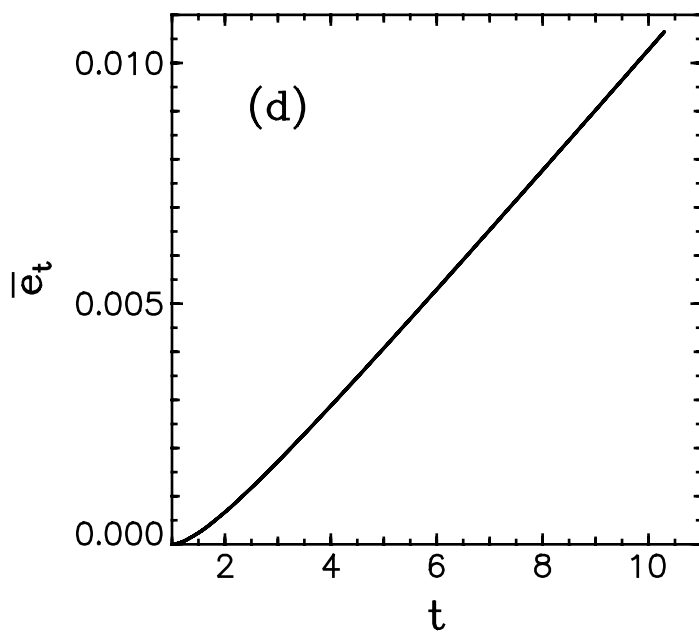
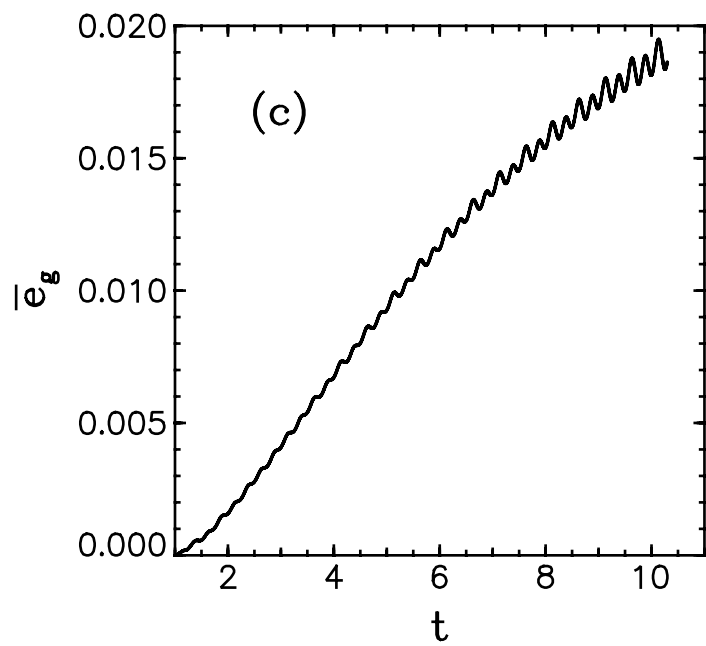
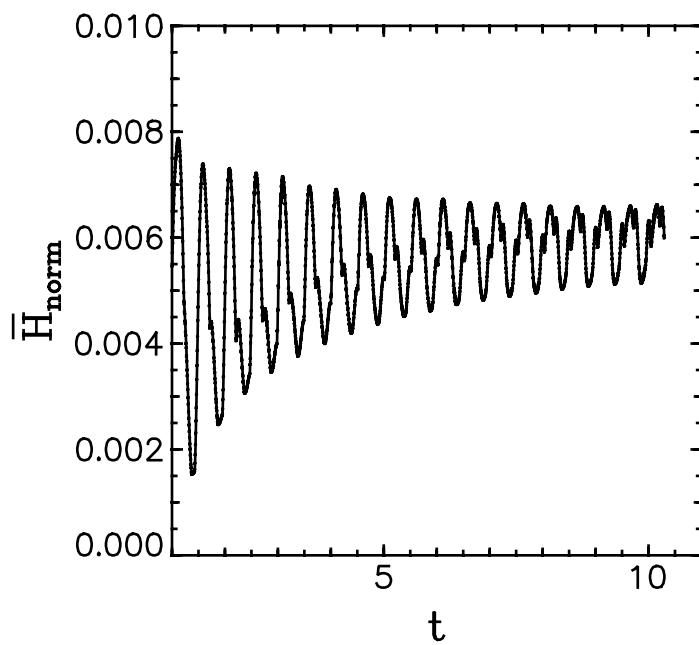
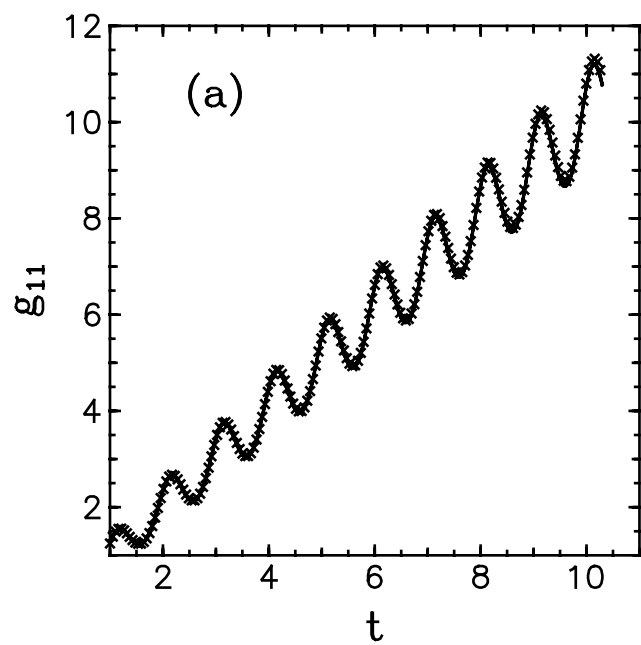


Figure 10

